Acoustics in a two-deck viscothermal boundary layer over an impedance surface

Doran Khamis & Edward James Brambley
DAMTP, University of Cambridge, Cambridge, CB3 0WA, United Kingdom

Published in the AIAA Journal, doi:10.2514/1.J055598

The acoustics of a mean flow boundary layer over an impedance surface or acoustic lining are considered. By considering a thick mean flow boundary layer (possibly due to turbulence), the boundary layer structure is separated asymptotically into two decks, with a thin weakly viscous mean flow boundary layer and an even thinner strongly viscous acoustic sublayer, without requiring a high-frequency. Using this, analytic solutions are found for the acoustic modes in a cylindrical lined duct. The mode shapes in each region compare well with numerical solutions of the linearised compressible Navier–Stokes equations, as does a uniform composite asymptotic solution. A closed-form effective impedance boundary condition is derived which can be applied to acoustics in inviscid slipping flow to account for both shear and viscosity in the boundary layer. The importance of the boundary layer is demonstrated in the frequency domain, and the new boundary condition is found to correctly predict the attenuation of upstream-propagating cuton modes, which are poorly predicted by existing inviscid boundary conditions. Stability is also investigated, and the new boundary condition is found to yield good results away from the critical layer. A time-domain formulation of a simplified version of the new impedance boundary condition is proposed.

1. Introduction

The generation and propagation of sound in an aeroengine is an increasingly important topic of research as air traffic increases and noise pollution regulations become more stringent. An important feature in the reduction of fan and engine noise is the inclusion of sections of acoustic lining at the intake or exhaust of an aeroengine. Usually, these acoustic linings are made of a honeycomb of small resonators designed to dampen tonal noise. Alternatively, bulk linings (e.g. foam or wool-type materials) can dampen broadband noise. Accurate theoretical modelling is essential to enable further optimisation of acoustic linings for future aircraft.

The majority of work pertaining to the acoustics above an acoustic lining considers an inviscid fluid. Early work considered a uniform flow [1, 2] or mean flow shear [3–5] and used numerical solutions of the linearised inviscid governing equations. More recent studies have shown that viscosity must be taken into account to accurately reproduce experimental results [6, 7].

Flow over acoustic linings also supports surface waves [8]. Analytical studies of a sheared inviscid boundary layer above an acoustic lining have led to revised predictions of the number of possible surface modes [9]. Stability analyses have shown that it is these surface modes that can lead to convective instabilities [9–11] that have also been identified in experiments [12, 13]. Because acoustic liners can support surface modes where a hard wall can not, their use could lead to generation or amplification of noise due to an instability being triggered. Theoretical identification of these unstable modes is therefore of utmost importance. It is known that viscosity effects the stability behaviour of surface modes, and stabilises the system at small wavelengths [14], but compared to the inviscid case, surface waves in the viscous case have received far less attention.

Viscosity has been included in a number of studies [15–17] aimed at deriving an effective impedance boundary condition that accounts for viscosity and shear in the boundary layer and may be applied at the wall of a uniform inviscid flow. In order to arrive at closed-form analytical solutions, these studies all make

simplifying assumptions. Nayfeh [15] considers only the acoustic boundary layer which is thin compared to the main flow boundary layer. In the study by Aurégan et al. [16], only small changes in the velocity and temperature are allowed across the boundary layer. Brambley [17] makes fewer simplifications but derives a system which models a vanishingly thin shear layer and which must be solved numerically; closed-form solutions are found only in a high frequency limit. This was extended to account for finite thickness effects by Khamis and Brambley [18], but again with no closed-form solution except in the high-frequency limit.

Without either making limiting simplifications or taking specific asymptotic limits, there is no known closed-form solutions for the acoustics in a finite-thickness sheared, viscous boundary layer. For high Reynolds number laminar flow over a rigid surface, mean flow viscous and thermal effects are expected near the boundary within a distance of order $\delta^* = \ell^*\sqrt{\nu^*/U^*\ell^*} = \ell^*/\sqrt{M\mathrm{Re}}$ given by Blasius theory, while acoustic viscous and thermal effects are expected near the boundary within a distance of order $\delta_a^* = \sqrt{\nu^*/\Omega^*} = \ell^*/\sqrt{\omega\mathrm{Re}}$, where ℓ^* is a relevant lengthscale, ν^* is the kinematic viscosity, U^* is the mean flow velocity, Ω^* is the acoustic frequency, $M = U^*/c^*$ is the Mach number, $\mathrm{Re} = c^*\ell^*/\nu^*$ is the Reynolds number based on the sound speed c^*, and $\omega = \Omega^*\ell^*/c^*$ is the Helmholtz number. The acoustic boundary layer is therefore much thinner than a laminar Blasius mean flow boundary layer only in the high frequency limit $\omega \gg 1$. However, reports of boundary layer thicknesses and Reynolds numbers in experimental studies suggest that the boundary layer momentum thickness is $\delta_m \approx 0.05$m in an aeroengine intake 2m in diameter at $\mathrm{Re}_c \approx 2\times10^7$ (defined by the centreline speed of sound) or $\mathrm{Re}_u \approx 7\times10^6$ (defined by the free stream fluid velocity), so that the boundary layer is thicker than would be predicted assuming a laminar Blasius boundary layer [6, 13]. This could be, for example, due to a turbulent boundary layer where the eddy viscosity (which governs the mean flow) is larger than the molecular viscosity (which is assumed here to govern viscous dissipation for acoustics). This work seeks to exploit this difference in viscous lengthscales in order to derive analytical solutions for the acoustics via matched asymptotic expansions in three scaling regions (an outer region and two boundary layer "decks") that cover an entire cylindrical, acoustically lined duct.

As is common in acoustics, in this paper we work predominantly in the frequency domain. The results of such work are not always directly applicable to time-domain numerical solvers. Recent work has made progress in implementing an inviscid impedance boundary condition in the time domain to account for a finite region of shear [19]. By incorporating the modified Myers boundary condition (reformulated in the time domain) into a linearised Euler solver, the unphysical numerical instabilities associated with time-domain formulations of the ill-posed classical Ingard–Myers boundary condition can be avoided. The physical surface wave instability is always present in the inviscid case [20], however, so the time-domain implementation in Brambley and Gabard [19] still yields instabilities. In the present work, we suggest a time-domain formulation that accounts for viscothermal effects in a thin, sheared boundary layer. Although the boundary condition is not implemented here, it is hoped that the good frequency-domain stability behaviour translates to a stable time-domain boundary condition, provided it is suitably implemented [19] and the boundary layer thickness and Reynolds number are chosen appropriately.

2. Governing equations

We consider the dynamics of a viscous, compressible perfect gas with pressure p^*, velocity $\mathbf{u}^* = (u^*, v^*, w^*)$, density ρ^*, temperature T^* and entropy s^*. These are governed by the Navier–Stokes equations,

$$\frac{\partial\rho^*}{\partial t^*} + \nabla^*\cdot(\rho^*\mathbf{u}^*) = 0, \tag{1a}$$

$$\rho^*\frac{D\mathbf{u}^*}{Dt^*} = -\nabla^* p^* + \nabla^*\cdot\sigma^*, \tag{1b}$$

$$\rho^* T^*\frac{Ds^*}{Dt^*} = \rho^* c_p^*\frac{DT^*}{Dt^*} - \frac{Dp^*}{Dt^*} = \nabla^*\cdot(\kappa^*\nabla^* T^*) + \sigma_{ij}^*\frac{\partial u_i^*}{\partial x_j^*}, \tag{1c}$$

$$\frac{\gamma}{\gamma-1}p^* = c_p^*\rho^* T^*, \tag{1d}$$

where $D/Dt^* = \partial/\partial t^* + \mathbf{u}^*.\nabla^*$ is the material derivative; $\gamma = c_p^*/c_v^*$ is the ratio of specific heats; and

$$\sigma_{ij}^* = 2\mu^*\left(\frac{\partial u_i^*}{\partial x_j^*} + \frac{\partial u_j^*}{\partial x_i^*}\right) + \mu_S^*\nabla^*\cdot\mathbf{u}^*\delta_{ij}. \tag{2}$$

is the viscous stress tensor. Here, κ^* is the thermal conductivity, μ^* the shear viscosity, and $\mu_S^* = \mu_B^* - 2\mu^*/3$ the second [21] viscosity, with μ_B^* the bulk viscosity. We consider a cylindrical duct in the coordinate system (x^*, r^*, θ), with a constant uniform base flow at its centreline $r^* = 0$. With a subscript 0 denoting values at the duct centreline, we nondimensionalise as follows: lengths are scaled by the duct radius l^*; velocity by the centreline speed of sound $c_0^* = \sqrt{\gamma p_0^*/\rho_0^*}$; time by l^*/c_0^*; density by ρ_0^*; pressure by $\rho_0^* {c_0^*}^2$; and temperature by ${c_0^*}^2/c_p^*$. The coefficients of viscosity are nondimensionalised by $c_0^* l^* \rho_0^*$, and the thermal conductivity by $c_0^* l^* \rho_0^* c_p^*$.

A. Linearized Acoustics

We linearise about a parallel base flow $\mathbf{U} = (U(r), 0, 0)$, which takes the nondimensional value $U_0 = M$, the centreline Mach number, in the core of the duct. The base pressure is assumed constant across the duct cross-section due to this choice of base flow, and takes the nondimensionalised value $p \equiv p_0 = 1/\gamma$; the centreline density and temperature are $\rho_0 = 1$ and $T_0 = 1/(\gamma - 1)$ respectively in this nondimensionalisation scheme. The equation of state (1d) couples the base temperature and density profiles as $(\gamma - 1)T(r) = 1/\rho(r)$. Small, unsteady acoustic perturbations are added to the mean flow in the form

$$Q_{\mathrm{tot}}(x, r, \theta, t) = Q(r) + \epsilon_a q'(x, r, \theta, t), \tag{3}$$

where $\epsilon_a \ll 1$ is the acoustic amplitude. Here, a prime denotes an acoustic perturbation in the time domain. We move to the frequency domain by defining the time-harmonic form $q'(x, r, \theta, t) = q(x, r, \theta) \exp(i\omega t)$, for frequency ω. Then, we look for modal acoustics of the form $q(x, r, \theta) = \tilde{q}(r) \exp(-ikx - im\theta)$, where k and m are the axial wavenumber and azimuthal mode number, respectively. Neglecting terms of $\mathcal{O}(\epsilon_a^2)$ or higher, the dimensionless linearised compressible Navier–Stokes (LNSE) equations may be written

$$\left.\begin{aligned}
&i\rho(\omega - Uk)\tilde{u} + \rho U_r \tilde{v} = ik\tilde{p} + \mathcal{V}^u, \qquad i\rho(\omega - Uk)\tilde{v} = -\tilde{p}_r + \mathcal{V}^v, \\
&i\rho(\omega - Uk)\tilde{w} = \frac{im}{r}\tilde{p} + \mathcal{V}^w, \qquad i\rho(\omega - Uk)\tilde{T} + \rho T_r \tilde{v} = i(\omega - Uk)\tilde{p} + \mathcal{V}^t, \\
&i\rho(\omega - Uk)\gamma\tilde{p} - i\rho^2(\omega - Uk)(\gamma - 1)\tilde{T} - ik\rho\tilde{u} + (\rho\tilde{v})_r + \frac{1}{r}\rho\tilde{v} - \frac{im}{r}\rho\tilde{w} = 0.
\end{aligned}\right\} \tag{4}$$

The viscous terms are collected in the $\mathcal{V}^i$ terms, and are defined by

$$\begin{aligned}
\mathcal{V}^u = \frac{(\gamma-1)}{\mathrm{Re}}\Big\{ &(T\tilde{u}_r + U_r\tilde{T})_r + \frac{1}{r}(T\tilde{u}_r + U_r\tilde{T}) - (2+\beta)k^2 T\tilde{u} - \frac{m^2}{r^2}T\tilde{u} \\
&- ik(1+\beta)(T\tilde{v})_r + ik\beta T_r\tilde{v} - \frac{ik}{r}(1+\beta)T\tilde{v} - \frac{km}{r}(1+\beta)T\tilde{w}\Big\},
\end{aligned} \tag{5a}$$

$$\begin{aligned}
\mathcal{V}^v = \frac{(\gamma-1)}{\mathrm{Re}}\Big\{ &- ik(1+\beta)(T\tilde{u})_r + ik(T_r\tilde{u} - U_r\tilde{T}) + (2+\beta)(T\tilde{v}_r)_r - \Big(k^2 + \frac{m^2}{r^2}\Big)T\tilde{v} \\
&- \frac{2}{r}T_r\tilde{v} + (2+\beta)\Big(\frac{T\tilde{v}}{r}\Big)_r - im(1+\beta)\Big(\frac{T\tilde{w}}{r}\Big)_r + \frac{im}{r}T_r\tilde{w} + \frac{2im}{r^2}T\tilde{w}\Big\},
\end{aligned} \tag{5b}$$

$$\begin{aligned}
\mathcal{V}^w = \frac{(\gamma-1)}{\mathrm{Re}}\Big\{ &- \frac{km}{r}(1+\beta)T\tilde{u} - \frac{im}{r^2}(3+\beta)T\tilde{v} - \frac{im}{r}(1+\beta)(T\tilde{v})_r + \frac{im}{r}\beta T_r\tilde{v} \\
&- \Big(k^2 + \frac{m^2}{r^2}\Big)T\tilde{w} + (T\tilde{w}_r)_r - \frac{m^2}{r^2}(1+\beta)T\tilde{w} + T\Big(\frac{\tilde{w}}{r}\Big)_r - \frac{1}{r}T_r\tilde{w}\Big\},
\end{aligned} \tag{5c}$$

$$\begin{aligned}
\mathcal{V}^t = \frac{(\gamma-1)}{\mathrm{Re}}\Big\{ &\frac{1}{\mathrm{Pr}}(T\tilde{T})_{rr} + \frac{1}{\mathrm{Pr}\,r}(T\tilde{T})_r - \frac{1}{\mathrm{Pr}}\Big(k^2 + \frac{m^2}{r^2}\Big)T\tilde{T} + U_r^2\tilde{T} + 2TU_r\tilde{u}_r \\
&- 2ikTU_r\tilde{v}\Big\}.
\end{aligned} \tag{5d}$$

The viscosities and thermal conductivity are taken to be linearly dependent on the temperature:

$$\mu = \frac{T}{T_0 \mathrm{Re}}, \qquad \mu_B = \frac{T}{T_0 \mathrm{Re}}\frac{\mu_0^{B*}}{\mu_0^*}, \qquad \kappa = \frac{T}{T_0 \mathrm{RePr}}. \tag{6}$$

The Reynolds number Re and the Prandtl number Pr are defined in terms of the centreline variables as

$$\mathrm{Re} = \frac{c_0^* l^* \rho_0^*}{\mu_0^*}, \qquad \mathrm{Pr} = \frac{\mu_0^* c_p^*}{\kappa_0^*}. \tag{7}$$

Note that Re is defined in terms of the centreline sound speed, and not the centreline fluid velocity, although $M\mathrm{Re} = \mathrm{Re}_u$ where $0 < M < 1$ is the Mach number, and so the two Reynolds numbers are of the same order of magnitude. We aim to solve (4) in the sheared boundary layer above an impedance lining, without assuming a high- or low-frequency approximation.

B. Solution outside the boundary layer

Close to the wall of a lined duct, a thin sheared boundary layer exists where viscosity may be important [6, 22]. Outside the boundary layer, where the base flow is constant, viscous effects may be regarded as negligible [14]. In the inviscid limit, (4) reduce to the linearised Euler equations from which for uniform flow Bessel's equation for the acoustic pressure may be derived:

$$\frac{\mathrm{d}^2\tilde{p}}{\mathrm{d}r^2} + \frac{1}{r}\frac{\mathrm{d}\tilde{p}}{\mathrm{d}r} + \left((\omega - Mk)^2 - k^2 - \frac{m^2}{r^2}\right)\tilde{p} = 0, \tag{8}$$

where the base flow takes its centreline values $U(r) \equiv M$, $\rho(r) \equiv 1$. Equation (8) may be solved in terms of Bessel functions, and the Euler momentum equation $i\rho(\omega - Uk)\tilde{v} = -\tilde{p}_r$ may be used to find the acoustic radial velocity,

$$\tilde{p}_{\mathrm{u}} = EJ_m(\alpha r), \qquad \tilde{v}_{\mathrm{u}} = \frac{iE\alpha J_m'(\alpha r)}{\omega - Mk}, \tag{9}$$

where $\alpha^2 = (\omega - Mk)^2 - k^2$, the subscript u denotes a solution in the uniform inviscid flow, and the amplitude E is an arbitrary constant. The relations (9) allow us to form an analytical expression for the effective impedance that the inviscid uniform flow solution sees at the wall,

$$Z_{\mathrm{eff}} = \frac{\tilde{p}_{\mathrm{u}}(1)}{\tilde{v}_{\mathrm{u}}(1)} = (\omega - Mk)\frac{J_m(\alpha)}{i\alpha J_m'(\alpha)}. \tag{10}$$

We are interested in how the physics of the boundary layer connects the actual boundary impedance $\tilde{p}/\tilde{v} = Z$ to the effective impedance Z_{eff} seen by the inviscid uniform-flow acoustics.

3. Main boundary layer solution

It is thought that the Reynolds number of the flow in an aeroengine bypass duct is between 10^5 and 10^7 in-flight, and at takeoff and landing [23]. Common assumptions for the thickness δ of the boundary layer are between 0.2 and 3% of the duct radius [24]. Experimental studies generally use fully-developed turbulent boundary layers, and are a useful benchmark for choices of parameter values. In one such study, Renou and Aurégan [6] report a Reynolds number of 3.38×10^5 (by the current definition); the boundary layer displacement (δ_d) and momentum (δ_m) thicknesses may be deduced from the data given in the reference to be $\delta_d \approx 5.1\%$ and $\delta_m \approx 3.9\%$ of the duct radius. The authors also give measurements of the (frequency dependent) acoustic boundary layer thickness, which lies in the range 0.26–0.67% of the duct radius, and is therefore far thinner than the mean flow boundary layer. In another study, Marx et al. [13] report $\mathrm{Re} \approx 2.4 \times 10^5$ (by the current definition); the boundary layer parameters were $\delta_d \approx 9\%$ and $\delta_m \approx 5\%$ of the duct radius. Assuming a laminar Blasius boundary layer gives the scaling $\delta \sim 1/\sqrt{\mathrm{Re}}$; this choice of scaling generally underestimates the boundary layer thickness in aeroengines, possibly due to the boundary layer being turbulent. We propose the new scaling $\delta \sim \mathrm{Re}^{-1/3}$, which models a slightly thicker boundary layer (or a slightly weaker viscosity) and is more in keeping with the scalings found in practice, as listed in table 1. Note, however, that we do not in any way model turbulence here.

The explicit boundary layer scaling used here is

$$r = 1 - \delta y, \qquad \xi\delta^3 = 1/\mathrm{Re}, \tag{12}$$

with $\xi = \mathcal{O}(1)$. The governing equations (4) are expanded in this regime, where y is the boundary layer variable. As in Brambley [17], the axial acoustic velocity and acoustic temperature perturbation are scaled as

$$\tilde{u} = \frac{\hat{u}}{\delta}, \qquad \tilde{T} = \frac{\hat{T}}{\delta} \tag{13}$$

Re \ δ	0.2%	1%	3%
10^5	2.5 : 1250	0.1 : 10	0.01 : 0.4
10^6	0.25 : 125	0.01 : 1	0.001 : 0.04
10^7	0.025 : 12.5	0.001 : 0.1	0.0001 : 0.004

Table 1. Values of ξ_b:ξ_c where $\xi_b = 1/\mathrm{Re}\delta^2$ is the Blasius scaling parameter, and $\xi_c = 1/\mathrm{Re}\delta^3$ is the parameter for the new scaling proposed here. A value of ξ close to unity indicates a pertinent scaling choice. Boundary layer thicknesses given as a percentage of duct radius.

to balance the leading order of the continuity equation. The governing equations to first order in δ are

$$i(\omega - Uk)\hat{T} + ikT\hat{u} + T^2\left(\frac{\tilde{v}}{T}\right)_y = \delta\left[\gamma i(\omega - Uk)T\tilde{p} + T\tilde{v} - imT\tilde{w}\right], \tag{14a}$$

$$i(\omega - Uk)\hat{u} - U_y\tilde{v} = \delta\left[\xi(\gamma-1)^2T(T\hat{u}_y + U_y\hat{T})_y + i(\gamma-1)kT\tilde{p}\right], \tag{14b}$$

$$\tilde{p}_y = \delta\frac{i(\omega - Uk)}{(\gamma-1)T}\tilde{v}, \tag{14c}$$

$$\frac{i(\omega - Uk)}{(\gamma-1)^2T}\tilde{w} = \frac{im}{\gamma-1}\tilde{p} + \mathcal{O}(\delta), \tag{14d}$$

$$\begin{aligned} i(\omega - Uk)\hat{T} - T_y\tilde{v} = \delta\Big[&\frac{1}{\mathrm{Pr}}\xi(\gamma-1)^2T(T\hat{T})_{yy} + \xi(\gamma-1)^2T(U_y^2\hat{T} + 2TU_y\hat{u}_y) \\ &+(\gamma-1)i(\omega - Uk)T\tilde{p}\Big]. \end{aligned} \tag{14e}$$

It is clear from (14) that the choice of scaling (12) has pushed viscosity back to being a first order effect. This has the advantage that the leading order solution is exactly the inviscid uniform solution, with the correction at $O(\delta)$ including both shear and viscothermal corrections.

To solve the system (14) we expand the acoustic quantities in powers of δ: $\tilde{q} = \tilde{q}_0 + \delta\tilde{q}_1 + \mathcal{O}(\delta^2)$. At leading order, we use the relations

$$\hat{u}_0 = -\frac{iU_y}{\omega - Uk}\tilde{v}_0, \qquad \hat{T}_0 = -\frac{iT_y}{\omega - Uk}\tilde{v}_0 \tag{15}$$

from (14b) and (14e) to rearrange the continuity equation (14a). The continuity equation reduces to

$$T(\omega - Uk)\left(\frac{\tilde{v}_0}{\omega - Uk}\right)_y = 0, \tag{16}$$

which has the solution $\tilde{v}_{\mathrm{m},0} = \bar{A}_0(\omega - Uk)$, where $\bar{A}_0$ is a constant and the subscript $\mathrm{m},0$ denotes the leading order of the main boundary layer. Thus we may write $\hat{u}_{\mathrm{m},0} = -iU_y\bar{A}_0$ and $\hat{T}_{\mathrm{m},0} = -iT_y\bar{A}_0$. The pressure equation (14c) is readily integrated at leading order to produce $\tilde{p}_{\mathrm{m},0} = \bar{P}_0$, a constant. We may use this in equation (14d) to find $\tilde{w}_{\mathrm{m},0} = m(\gamma-1)T\bar{P}_0/(\omega - Uk)$. This is the highest order of the azimuthal acoustic velocity solution that we need for the current study.

At first order, the $\hat{u}$ and $\hat{T}$ solutions may be written

$$\hat{u}_{\mathrm{m},1} = -\frac{iU_y}{\omega - Uk}\tilde{v}_{\mathrm{m},1} + \frac{(\gamma-1)kT}{\omega - Uk}\bar{P}_0 - \xi\bar{A}_0\frac{(\gamma-1)^2T}{\omega - Uk}(U_yT)_{yy}, \tag{17}$$

$$\hat{T}_{\mathrm{m},1} = -\frac{iT_y}{\omega - Uk}\tilde{v}_1 + (\gamma-1)T\bar{P}_0 - \xi\bar{A}_0\frac{(\gamma-1)^2T}{\omega - Uk}\left(\frac{1}{2\mathrm{Pr}}(T^2)_{yyy} + (TU_y^2)_y\right), \tag{18}$$

where the subscript 1 denotes the first order. These are used in (14a) which, when integrated, gives

$$\begin{aligned} \tilde{v}_{\mathrm{m},1} = &\bar{A}_1(\omega - Uk) + \bar{A}_0(\omega - Uk)y + i\bar{P}_0(\omega - Uk)y\Big(1 - \frac{k^2+m^2}{(\omega - Mk)^2}\Big) \\ &+ i\bar{P}_0(\omega - Uk)\frac{k^2+m^2}{(\omega - Mk)^2}\int_0^y \chi_1\,\mathrm{d}y + i\xi\bar{A}_0(\gamma-1)^2(\omega - Uk)\int_0^y \bar{\chi}_\mu\,\mathrm{d}y, \end{aligned} \tag{19}$$

where $\bar{A}_1$ is a constant, and

$$\chi_1 = 1 - \frac{(\omega - Mk)^2}{\rho(\omega - Uk)^2}, \qquad \bar{\chi}_\mu = \frac{1}{\omega - Uk}\left(\frac{1}{2\mathrm{Pr}}(T^2)_{yyy} + (TU_y^2)_y + \frac{kT}{\omega - Uk}(U_y T)_{yy}\right). \tag{20}$$

Note that viscous terms, identifiable by the parameter ξ, have arisen at this order in eqs. (17)–(19). The first order pressure is found by integrating (14c):

$$\tilde{p}_{\mathrm{m},1} = \bar{P}_1 + i\bar{A}_0(\omega - Mk)^2 y - i\bar{A}_0(\omega - Mk)^2 \int_0^y \chi_0 \,\mathrm{d}y, \tag{21}$$

where $\bar{P}_1$ is a constant, and

$$\chi_0 = 1 - \frac{\rho(\omega - Uk)^2}{(\omega - Mk)^2}. \tag{22}$$

In summary, the solutions for the acoustic pressure and radial velocity in the main boundary layer, correct to first order, are

$$\begin{aligned}\tilde{v}_{\mathrm{m}} = (\omega - Uk)\Bigg\{ &\bar{A}_0 + \delta\bar{A}_1 + \delta\bar{A}_0 y + i\delta\bar{P}_0 y\Big(1 - \frac{k^2 + m^2}{(\omega - Mk)^2}\Big) \\ &+ i\delta\bar{P}_0 \frac{k^2 + m^2}{(\omega - Mk)^2}\int_0^y \chi_1 \,\mathrm{d}y + i\delta\xi\bar{A}_0(\gamma - 1)^2 \int_0^y \bar{\chi}_\mu \,\mathrm{d}y\Bigg\},\end{aligned} \tag{23a}$$

$$\tilde{p}_{\mathrm{m}} = \bar{P}_0 + \delta\bar{P}_1 + i\delta\bar{A}_0(\omega - Mk)^2 y - i\delta\bar{A}_0(\omega - Mk)^2 \int_0^y \chi_0 \,\mathrm{d}y. \tag{23b}$$

These are identical in form to the pressure and radial velocity found by Brambley [10] by assuming an inviscid, thin-but-nonzero thickness boundary layer — but for the addition of the viscous integral $\bar{\chi}_\mu$ at first order in $\tilde{v}$. The constants $\bar{A}_0$, $\bar{A}_1$, $\bar{P}_0$ and $\bar{P}_1$ will be found by matching to the outer solution as $y \to \infty$.

The axial and azimuthal velocities in this scaling regime do not satisfy no slip at the wall $y = 0$. We have not, therefore, captured the full viscous dynamics of the boundary layer. The solutions (23) should be viewed as the *less* viscous main boundary layer solution that sits atop a viscous acoustic sublayer, which will be considered in section 4.

A. Matching the main boundary layer solution to the outer flow

The acoustics in the outer flow to which we asymptotically match are the uniform flow acoustics (9) expanded near the boundary. These are, in the limit $r \to 1$,

$$\tilde{p}_{\mathrm{u}}(1 - \delta y) \sim p_\infty + \delta y i(\omega - Mk)v_\infty + \mathcal{O}(\delta^2), \tag{24a}$$

$$\tilde{v}_{\mathrm{u}}(1 - \delta y) \sim v_\infty - \delta y\left(\frac{(\omega - Mk)^2 - k^2 - m^2}{i(\omega - Mk)}p_\infty - v_\infty\right) + \mathcal{O}(\delta^2), \tag{24b}$$

where

$$p_\infty = EJ_m(\alpha), \qquad \text{and} \qquad v_\infty = \frac{i\alpha E J_m'(\alpha)}{(\omega - Mk)}. \tag{25}$$

We match (23) to (24) in the limit $y \to \infty$. At leading order we find

$$\bar{A}_0 = \frac{v_\infty}{\omega - Mk}, \qquad \bar{P}_0 = p_\infty. \tag{26}$$

At first order, we require the terms proportional to y in (23) to match with the outer solutions, while the constant terms should cancel. Thus,

$$\bar{A}_1 = -ip_\infty \frac{k^2 + m^2}{(\omega - Mk)^2} I_1 - \frac{i\xi(\gamma - 1)^2}{\omega - Mk} v_\infty \bar{I}_\mu, \tag{27a}$$

$$\bar{P}_1 = i(\omega - Mk)v_\infty I_0 \tag{27b}$$

where

$$I_0 = \int_0^\infty \chi_0 \,\mathrm{d}y, \qquad I_1 = \int_0^\infty \chi_1 \,\mathrm{d}y, \qquad \bar{I}_\mu = \int_0^\infty \bar{\chi}_\mu \,\mathrm{d}y. \tag{28}$$

The viscous integral (that of $\bar{\chi}_\mu$) is bounded as $y \to \infty$ because the gradients of the base flow are non-zero only inside the boundary layer.

B. Behaviour of the main boundary layer solutions near the boundary

Here we find the limiting behaviour of the solutions found in the previous section, (23), as $y \to 0$. This will be needed in section 4 when matching to the viscous sublayer solution. Expanding first the integrals, we find

$$\int_0^y \chi_0 \,\mathrm{d}y \sim \left(1 - \frac{\rho(0)\omega^2}{(\omega - Mk)^2}\right) y + \mathcal{O}(y^2), \tag{29a}$$

$$\int_0^y \chi_1 \,\mathrm{d}y \sim \left(1 - \frac{(\omega - Mk)^2}{\rho(0)\omega^2}\right) y + \mathcal{O}(y^2), \tag{29b}$$

$$\begin{aligned}\int_0^y \bar{\chi}_\mu \,\mathrm{d}y \sim \frac{y}{\omega^2}\Big(&kT(0)^2U'''(0) + kT(0)T''(0)U'(0) + 2\omega T(0)U'(0)U''(0) \\ &+ \frac{\omega}{\mathrm{Pr}}T(0)T'''(0)\Big) + \mathcal{O}(y^2),\end{aligned} \tag{29c}$$

where we assume the base flow is non-slipping and satisfies isothermal wall conditions, $U(0) = 0$ and $T'(0) = 0$, such that $U(y) \sim U'(0)y$ and $T(y) \sim T(0)$, and similar for their derivatives. A prime denotes a derivative with respect to y. Thus for small y the pressure and velocity behave as

$$\begin{aligned}\tilde{v}_\mathrm{m}^{(I)} \sim{}& \bar{A}_0\left(\omega - U'(0)ky - \frac{1}{2}U''(0)ky^2\right) + \delta\bar{A}_1(\omega - U'(0)ky) + \delta\bar{A}_0\omega y + i\delta y\bar{P}_0\omega \\ &- i\delta y\bar{P}_0\frac{k^2+m^2}{\rho(0)\omega} + i\delta y\xi\bar{A}_0(\gamma-1)^2\omega\Big(\frac{k}{\omega^2}T(0)^2U'''(0) + \frac{k}{\omega^2}T(0)T''(0)U'(0) \\ &+ \frac{2}{\omega}T(0)U'(0)U''(0) + \frac{1}{\mathrm{Pr}\omega}T(0)T'''(0)\Big) + \mathcal{O}(\delta^2, \delta y^2, y^3),\end{aligned} \tag{30a}$$

$$\tilde{p}_\mathrm{m}^{(I)} \sim \bar{P}_0 + \delta\bar{P}_1 + i\delta y\bar{A}_0\rho(0)\omega^2 + \mathcal{O}(\delta^2, \delta y^2). \tag{30b}$$

These forms, (30), will be used as the outer solutions to which the viscous sublayer solutions, derived in the next section, should match.

4. Viscous sublayer solution

We assume the existence of a thin viscous sublayer within which the base flow does not change quickly, but the acoustics change rapidly enough to satisfy viscous wall conditions at $r = 1$, $y = 0$. We scale into this sublayer by

$$y = \varepsilon z, \qquad \varepsilon = \sqrt{\delta/\omega} \sim \mathrm{Re}^{-1/6}, \tag{31}$$

as described in appendix A. Note that this does not assume high frequency (large ω), although this scaling would break down for very small frequencies $\omega \lesssim \delta$. We may expand the base flow near the wall using the no slip and isothermal wall conditions,

$$\begin{aligned}U \sim{}& \varepsilon zU'(0) + \frac{1}{2}\varepsilon^2z^2U''(0), \qquad U_y \sim U'(0) + \varepsilon zU''(0) + \frac{1}{2}\varepsilon^2z^2U'''(0), \\ U_{yy} \sim{}& U''(0) + \varepsilon zU'''(0) + \frac{1}{2}\varepsilon^2z^2U''''(0), \qquad T \sim T(0) + \frac{1}{2}\varepsilon^2z^2T''(0), \\ T_y \sim{}& \varepsilon zT''(0) + \frac{1}{2}\varepsilon^2z^2T'''(0), \qquad T_{yy} \sim T''(0) + \varepsilon zT'''(0) + \frac{1}{2}\varepsilon^2z^2T''''(0),\end{aligned} \tag{32}$$

where the derivatives and arguments of the base flow variables remain in terms of y, i.e.

$$U'(0) \equiv \left.\frac{\mathrm{d}}{\mathrm{d}y}U(y)\right|_{y=0}.$$

We will drop the argument 0 for all base flow variables in this section, as they will all be evaluated at the boundary: $U' \equiv U'(0)$, and so on.

Expanding (4) in powers of ε using (31) and (32) leads to the sublayer governing equations

$$\tilde{v}_z = \varepsilon\Big[-ik\hat{u} - \frac{i\omega}{T}\hat{T}\Big] + \varepsilon^2\Big[ik\frac{U'}{T}z\hat{T} + \frac{T''}{T}z\tilde{v}\Big] + \varepsilon^3\Big[(kU'' + \omega T'')\frac{i}{2T}z^2\hat{T} + \frac{T'''}{2T}z^2\tilde{v} - im\omega\tilde{w} + i\gamma\omega^2\tilde{p} + \omega\tilde{v}\Big], \tag{33a}$$

$$\hat{u}_{zz} - \eta^2\hat{u} = \frac{iU'}{\omega}\eta^2\tilde{v} - \varepsilon\Big[\frac{kU'}{\omega}\eta^2 z\hat{u} + \frac{U'}{T}\hat{T}_z - \frac{iU''}{\omega}\eta^2 z\tilde{v}\Big] - \varepsilon^2\Big[k\eta^2(\gamma-1)T\tilde{p} - \frac{iU'''}{2\omega}\eta^2 z^2\tilde{v} + \frac{kU''}{2\omega}\eta^2 z^2\hat{u} + \frac{T''}{T}(z^2\hat{u}_{zz} + z\hat{u}_z) + \frac{U''}{T}(z\hat{T})_z\Big], \tag{33b}$$

$$\tilde{p}_z = \varepsilon^3\Big[\frac{i\omega^2}{(\gamma-1)T}\tilde{v} - \frac{i\omega^2(2+\beta)}{(\gamma-1)\eta^2 T}\tilde{v}_{zz}\Big], \tag{33c}$$

$$\tilde{w}_{zz} - \eta^2\tilde{w} = -\frac{m}{\omega}(\gamma-1)T\eta^2\tilde{p} + \mathcal{O}(\varepsilon), \tag{33d}$$

$$\frac{1}{\mathrm{Pr}}\hat{T}_{zz} - \eta^2\hat{T} = -\varepsilon\Big[2U'\hat{u}_z + \frac{kU'}{\omega}\eta^2 z\hat{T} - \frac{iT''}{\omega}\eta^2 z\tilde{v}\Big] - \varepsilon^2\Big[(\gamma-1)T\omega\eta^2\tilde{p} - \frac{iT'''}{2\omega}\eta^2 z^2\tilde{v} + 2U''z\hat{u}_z + \frac{kU''}{2\omega}\eta^2 z^2\hat{T} + \frac{U'^2}{T}\hat{T} + \frac{1}{\mathrm{Pr}}\frac{T''}{T}\Big((z^2\hat{T}_z)_z + \hat{T}\Big)\Big], \tag{33e}$$

where we have defined

$$\eta^2 = \frac{i}{\xi(\gamma-1)^2T(0)^2} \tag{34}$$

with $\mathrm{Re}(\eta) > 0$. To find $\tilde{p}$ and $\tilde{v}$ to the desired order, we need to calculate $\hat{u}$ and $\hat{T}$ to $\mathcal{O}(\varepsilon^2)$ and $\tilde{w}$ to $\mathcal{O}(1)$. The system (33) may be solved by expanding the acoustic quantities in powers of ε, $q = q_0 + \varepsilon q_1$ *et cetera*; details of this solution may be found in appendix B. The main results are expressions for the pressure and radial velocity in the acoustic boundary layer to $\mathcal{O}(\varepsilon^3)$,

$$\tilde{p}_\mathrm{s}(z) = P_0 + \varepsilon P_1 + \varepsilon^2 P_2 + \varepsilon^3\Big(P_3 + \frac{i\omega^2}{(\gamma-1)T}A_0 z\Big), \tag{35a}$$

$$\tilde{v}_\mathrm{s}(z) = A_0 + \varepsilon\left[A_1 + a_0\mathrm{e}^{-\eta z} + a_1 z\right] + \varepsilon^2\Big[A_2 + a_2 z + a_3 z^2 + (a_4 + a_5 z + a_6 z^2)\mathrm{e}^{-\eta z} + a_7\mathrm{e}^{-\sigma\eta z}\Big] + \varepsilon^3\Big[A_3 + a_8 z + a_9 z^2 + a_{10}z^3 + (a_{11} + a_{12}z + a_{13}z^2 + a_{14}z^3 + a_{15}z^4)\mathrm{e}^{-\eta z} + (a_{16} + a_{17}z + a_{18}z^2)\mathrm{e}^{-\sigma\eta z}\Big], \tag{35b}$$

where A_j and P_j are constants of integration, and a_j are linear combinations of the A_j and P_j given in appendix B. Here, $\sigma = \sqrt{\mathrm{Pr}}$, and the subscript s denotes a solution in the viscous sublayer.

In the limit $z \to \infty$, $\tilde{p}$ and $\tilde{v}$ from (35) behave as

$$\tilde{p}_\mathrm{s} \sim P_0 + \varepsilon P_1 + \varepsilon^2 P_2 + \varepsilon^3\left(P_3 + \frac{i\omega^2}{(\gamma-1)T}A_0 z\right) + \mathcal{O}(\varepsilon^4), \tag{36a}$$

$$\tilde{v}_\mathrm{s} \sim A_0 + \varepsilon\left(A_1 + a_1 z\right) + \varepsilon^2\left(A_2 + a_2 z + a_3 z^2\right) + \varepsilon^3\left(A_3 + a_8 z + a_9 z^2 + a_{10}z^3\right) + \mathcal{O}(\varepsilon^4), \tag{36b}$$

where the exponentially small, necessarily viscous, terms in (35) vanish in this outer limit. We now match to the main boundary layer solution.

An intermediate variable is introduced to facilitate matching: let

$$\tau = y/\varepsilon^\lambda = z\varepsilon^{1-\lambda} \tag{37}$$

where $0 < \lambda < 1$. We then take the limit $\varepsilon \to 0$, holding τ fixed. For the acoustic pressure, the main boundary layer solution in the limit $y \to 0$, (30b), and the sublayer solution in the limit $z \to \infty$, (36a), may be rewritten in terms of the intermediate variable τ using (37). We find, as $\varepsilon \to 0$,

$$\tilde{p}_\mathrm{m} \sim \bar{P}_0 + \varepsilon^2\omega\bar{P}_1 + i\varepsilon^{2+\lambda}\tau\omega^3\bar{A}_0\rho(0) + \mathcal{O}(\varepsilon^4, \varepsilon^{2+2\lambda}) \tag{38a}$$

$$\tilde{p}_\mathrm{s} \sim P_0 + \varepsilon P_1 + \varepsilon^2 P_2 + \varepsilon^{2+\lambda}\tau\frac{i\omega^2}{(\gamma-1)T(0)}A_0 + \varepsilon^3 P_3 + \mathcal{O}(\varepsilon^4, \varepsilon^{2+2\lambda}). \tag{38b}$$

Similarly, the $\tilde{v}$ expansion in the limit $\varepsilon \to 0$ with τ held fixed gives

$$\tilde{v}_{\mathrm{m}} \sim \omega\bar{A}_0 - \varepsilon^{\lambda}\tau k U'(0)\bar{A}_0 - \varepsilon^{2\lambda}\tau^2\frac{kU''(0)}{2}\bar{A}_0 - \varepsilon^{3\lambda}\tau^3\frac{kU'''(0)}{6}\bar{A}_0 + \varepsilon^2\omega^2\bar{A}_1 + \varepsilon^{2+\lambda}\tau\Bigg\{\omega^2\bar{A}_0 - kU'(0)\omega\bar{A}_1 + i\omega^2\bar{P}_0 - i\frac{k^2+m^2}{\rho(0)}\bar{P}_0 + i\xi(\gamma-1)^2T(0)^2\omega\bar{A}_0\Bigg(\frac{kU'''(0)}{\omega} + \frac{kT''(0)U'(0)}{\omega T(0)} + \frac{2U'(0)U''(0)}{T(0)} + \frac{1}{\mathrm{Pr}}\frac{T'''(0)}{T(0)}\Bigg)\Bigg\} + \mathcal{O}(\varepsilon^{2+2\lambda}, \varepsilon^{4\lambda}), \tag{39}$$

for the main boundary layer solution, and

$$\tilde{v}_{\mathrm{s}} \sim A_0 - \varepsilon^{\lambda}\tau\frac{kU'(0)}{\omega}A_0 + \varepsilon A_1 - \varepsilon^{2\lambda}\tau^2\frac{kU''(0)}{2\omega}A_0 - \varepsilon^{3\lambda}\tau^3\frac{kU'''(0)}{6\omega}A_0 - \varepsilon^{1+\lambda}\tau\frac{kU'(0)}{\omega}A_1 + \varepsilon^2 A_2 - \varepsilon^{1+2\lambda}\tau^2\frac{kU''(0)}{2\omega}A_1 + \varepsilon^{2+\lambda}\tau\Bigg\{\omega A_0 + i\omega^2 P_0 - i(k^2+m^2)(\gamma-1)T(0)P_0 - \frac{kU'(0)}{\omega}A_2 - \frac{1}{\eta^2}A_0\Bigg(\frac{T'''(0)}{\mathrm{Pr}T(0)} + \frac{2U'(0)U''(0)}{T(0)} + \frac{kT''(0)U'(0)}{\omega T(0)} + \frac{kU'''(0)}{\omega}\Bigg)\Bigg\} + \varepsilon^3 A_3 + \mathcal{O}(\varepsilon^4, \varepsilon^{2+2\lambda}) \tag{40}$$

for the sublayer solution. These equations must match independently of $\lambda \in (0,1)$.

We may identify from (38) that $P_0 = \bar{P}_0$ and $P_2 = \omega\bar{P}_1$. The $\mathcal{O}(\varepsilon)$ matching gives $P_1 = 0$. Because we want the matching to work for any value of the exponent $\lambda \in (0,1)$, we set $P_3 = 0$. From the leading order of (39) and (40) we can readily identify $A_0 = \omega\bar{A}_0$. This is consistent with higher order terms of (39) and (40), and also with the $\mathcal{O}(\varepsilon^{2+\lambda})$ terms in the $\tilde{p}$ expansions (38) once we write $\rho(0) = 1/(\gamma-1)T(0)$. At $\mathcal{O}(\varepsilon^2)$ we find $A_2 = \omega^2\bar{A}_1$. Due to the absence of ε and ε^3 terms in (39), we set $A_1 = A_3 = 0$. The remaining terms at $\mathcal{O}(\varepsilon^{2+\lambda})$ match if the definition of η is inserted from (34).

5. Results for the mode shapes

All results presented here use hyperbolic velocity and temperature profiles,

$$U(r) = M\tanh\left(\frac{1-r}{\delta}\right) + M\left(1 - \tanh\left(\frac{1}{\delta}\right)\right)\left(\frac{1+\tanh(1/\delta)}{\delta}r + (1+r)\right)(1-r) \tag{41a}$$

$$T(r) = T_0 + T_{\mathrm{w}}\left(\cosh\left(\frac{1-r}{\delta}\right)\right)^{-1}, \tag{41b}$$

where δ is a measure of boundary layer thickness, with $U(1-3\delta) \approx 0.995M$. For the results presented here, $T_{\mathrm{w}} = 0.104$.

A. Mode shapes in three scaling regions

First we show some examples of the acoustic mode shapes that result from the three different duct regions considered in the asymptotic analysis. The patchwork of regions of validity for the radial velocity can be seen in fig. 1: compared to the numerical solution of the full LNSE (for details of the numerical method see section 3 and appendix C of [18]), the uniform flow outer solution $\tilde{v}_{\mathrm{u}}$ is valid for most of the duct, where the shear is negligible (fig. 1a); the main boundary layer solution $\tilde{v}_{\mathrm{m}}$ is accurate where the mean flow shear is important, but loses accuracy very close to the wall (fig. 1b); the viscous sublayer solution $\tilde{v}_{\mathrm{s}}$ is accurate in the acoustic boundary layer very close to the wall (fig. 1c). Figure 2 shows the mode shape of the acoustic pressure for the same parameters — we see that the sublayer solution is indeed the inner expansion of the main boundary layer solution (see fig. 2c). For the axial velocity we see a similar thing (fig. 3), except here the viscous sublayer solution is significantly different from the main boundary layer solution due to the sublayer solution satisfying no slip at the wall.

B. Composite solutions

Here we derive solutions for the acoustic mode shapes that are uniformly valid in r. We have defined three regions of the duct: the outer region, where the base flow is uniform and inviscid; the main boundary

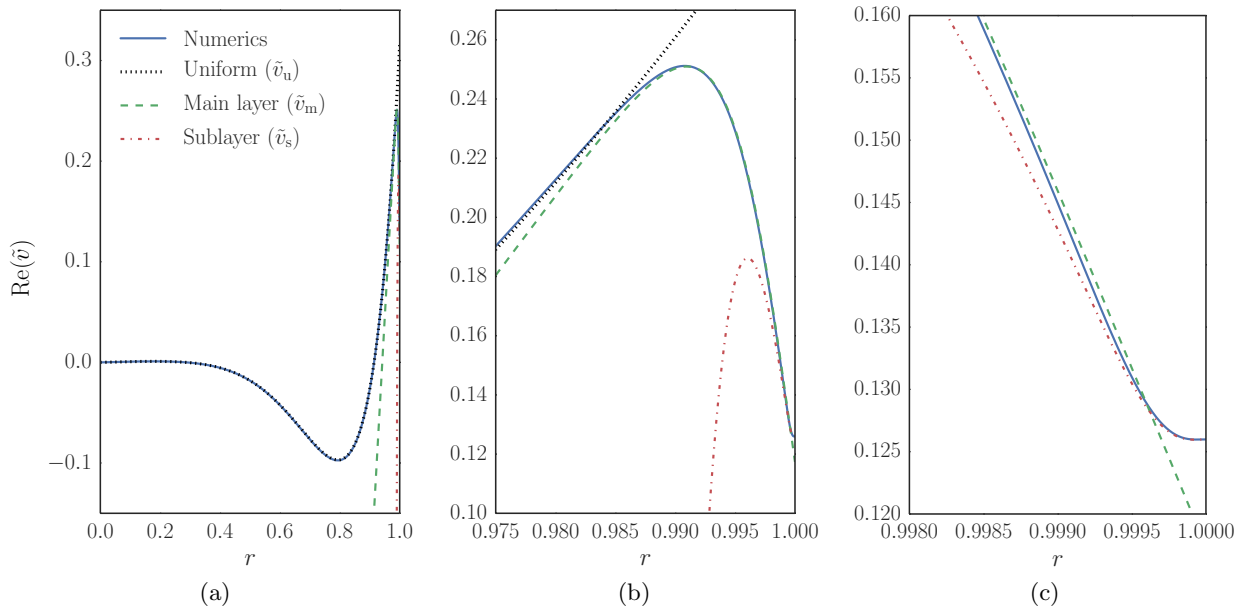

Figure 1. Acoustic mode shape for the radial velocity $\tilde{v}$ found by numerically solving the LNSE, with the three asymptotic solutions overlaid, showing their patchwork of regions of validity. (a) shows the full duct $r \in [0, 1]$, (b) shows the main boundary layer, (c) shows the viscous sublayer. Parameters are $\omega = 5$, $k = -14 + 5i$, $m = 0$, $M = 0.5$, $\delta = 6 \times 10^{-3}$, $\mathrm{Re} = 5 \times 10^6$.

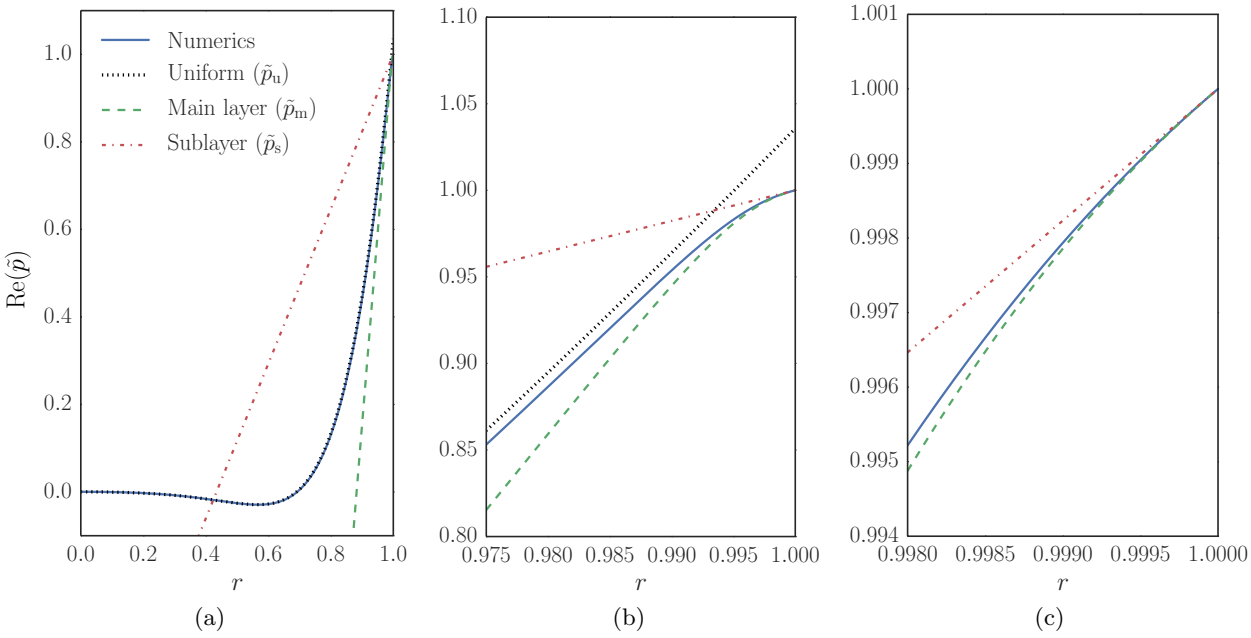

Figure 2. Acoustic mode shape for the acoustic pressure $\tilde{p}$ found by numerically solving the LNSE, with the three asymptotic solutions overlaid, showing their patchwork of regions of validity. (a) shows the full duct $r \in [0, 1]$, (b) shows the main boundary layer, (c) shows the viscous sublayer. Parameters as in fig. 1.

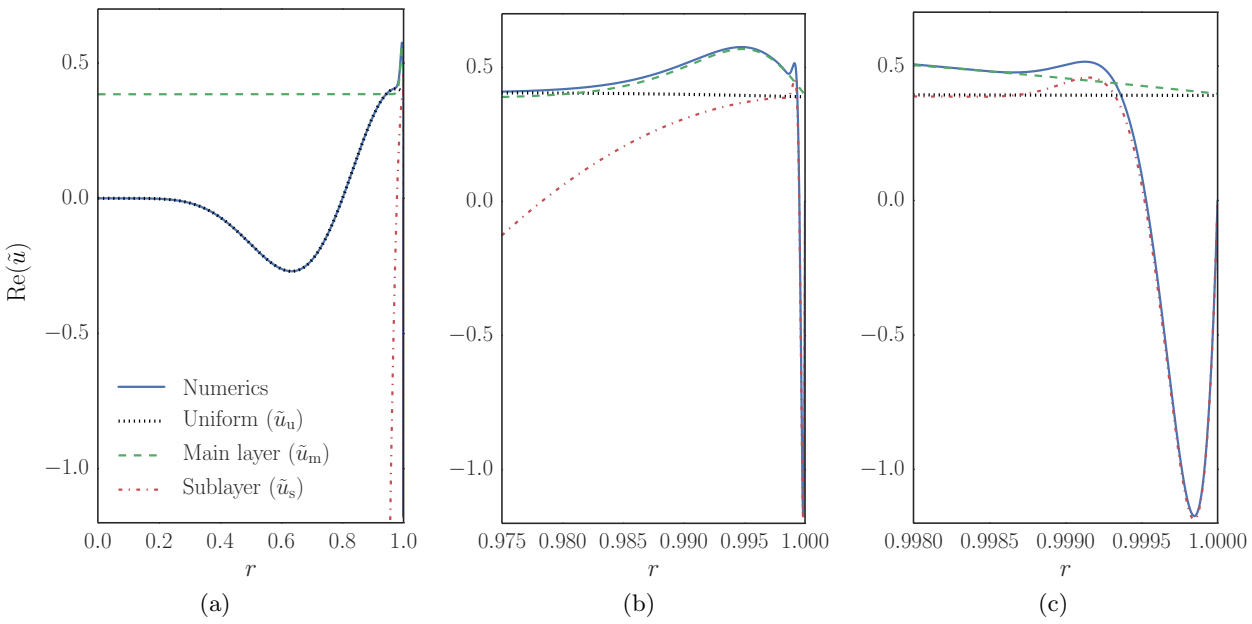

Figure 3. Acoustic mode shape for the axial velocity $\tilde{u}$ found by numerically solving the LNSE, with the three asymptotic solutions overlaid, showing their patchwork of regions of validity. (a) shows the full duct $r \in [0, 1]$, (b) shows the main boundary layer, (c) shows the viscous sublayer. Parameters are $\omega = 15$, $k = 5+2i$, $m = 6$, $M = 0.5$, $\delta = 7\times10^{-3}$, $\mathrm{Re} = 3\times10^{6}$.

layer, where the base flow is sheared and viscosity is a first order perturbation; and the sublayer, where the base flow varies slowly, and viscous and inertial effects balance to enforce no slip and isothermal boundary conditions at the wall. In the outer region, the Bessel function solutions defined in (9) hold; in the main boundary layer the expansions (23) hold; while in the sublayer the expansions (35) hold.

For the pressure, since the sublayer solution (35a) is inviscid to $\mathcal{O}(\varepsilon^3)$, it transpires that the sublayer solution is exactly the inner expansion of the main boundary layer solution (23b) for small y; this is why fig. 2c shows the main boundary layer solution continuing to perform well within the sublayer region. Thus, we need only form a composite of the outer solution $\tilde{p}_\mathrm{u} = EJ_m(\alpha r)$ and the main boundary layer solution. This is equivalent to that found by Brambley for the modified Myers boundary condition [10]. Using the definition of p_∞ from (25), the uniformly valid composite solution $\tilde{p}_c$, valid across all regions, is given by

$$\frac{\tilde{p}_c}{p_\infty} = \frac{J_m(\alpha r)}{J_m(\alpha)} - \frac{\alpha J'_m(\alpha)}{J_m(\alpha)} \int_0^r 1 - \frac{\rho(\omega - Uk)^2}{(\omega - Mk)^2} \mathrm{d}r. \tag{42}$$

Setting the amplitude of the wave, through the value of p_∞, is the only degree of freedom remaining in (42).

Turning to the radial velocity, we may write the sublayer solution (35b) as

$$\tilde{v}_\mathrm{s} = V_1(z;\varepsilon) + V_2(z;\varepsilon)\mathrm{e}^{-\eta z} + V_3(z;\varepsilon)\mathrm{e}^{-\sigma\eta z}. \tag{43}$$

Since the V_2 and V_3 terms decay exponentially as $z \to \infty$, and since theV_1 term is exactly the inner expansion of the main boundary layer solution $\tilde{v}_m$ (23a) for small y, a composite of the main boundary layer and sublayer solutions is given by $\tilde{v}_{cBL}$,

$$\tilde{v}_{cBL} = \tilde{v}_\mathrm{m} + V_2(z;\varepsilon)\mathrm{e}^{-\eta z} + V_3(z;\varepsilon)\mathrm{e}^{-\sigma\eta z}. \tag{44}$$

We form a full composite expansion by additive composing $\tilde{v}_{cBL}$ with the outer inviscid solution $\tilde{v}_\mathrm{u} = i\alpha p_\infty J'_m(\alpha r)/J_m(\alpha)(\omega - Mk)$, giving the full composite solution $\tilde{v}_c = \tilde{v}_\mathrm{u} + \tilde{v}_{cBL} - \tilde{v}_\mathrm{m}^{(O)}$, where $\tilde{v}_\mathrm{m}^{(O)}$ is the

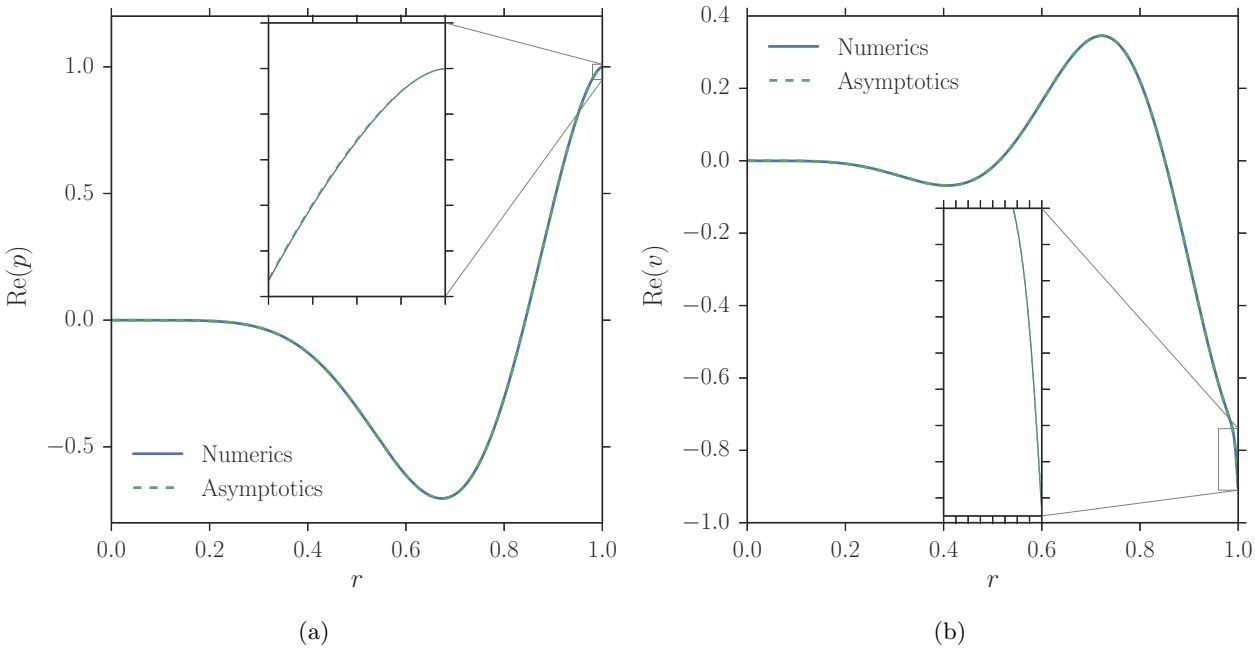

Figure 4. Comparison of the numerical LNSE mode shapes and the composite asymptotic mode shapes (42) and (45) for (a) the pressure $\tilde{p}$ and (b) the radial velocity $\tilde{v}$. Parameters are $\omega = 15$, $k = 5 + 2i$, $m = 6$, $M = 0.5$, $\delta = 7 \times 10^{-3}$, $\mathrm{Re} = 3 \times 10^{6}$. Inset axes show behaviour of solutions close to the wall at $r = 1$.

outer expansion as $y \to \infty$ of $\tilde{v}_\mathrm{m}$ given in (24b). In full, this composite solution is

$$\begin{aligned}\frac{\tilde{v}_c}{p_\infty} =& \frac{i}{\omega - Mk}\frac{\alpha J_m'(\alpha r)}{J_m(\alpha)} + ik\frac{(M-U)}{(\omega-Mk)^2}\left(\frac{\alpha J_m'(\alpha)}{J_m(\alpha)} + (1-r)\frac{\alpha J_m'(\alpha)}{J_m(\alpha)} + (1-r)(\alpha^2 - m^2)\right)\\ &+ \frac{(\omega - Uk)}{(\omega - Mk)^2}\left(\frac{(\gamma-1)^2}{\omega \mathrm{Re}}\frac{\alpha J_m'(\alpha)}{J_m(\alpha)}\int_0^r \frac{\chi_\mu(r)}{\delta^3}\mathrm{d}r - i(k^2+m^2)\int_0^r \chi_1(r)\mathrm{d}r\right)\\ &+ \frac{\bar{V}_2(z;\varepsilon)}{J_m(\alpha)}\mathrm{e}^{-\sqrt{i}(1-r)/\delta_\mathrm{ac}} + \frac{\bar{V}_3(z;\varepsilon)}{J_m(\alpha)}\mathrm{e}^{-\sqrt{i}\sigma(1-r)/\delta_\mathrm{ac}},\end{aligned} \tag{45}$$

where

$$\delta_\mathrm{ac} = \frac{(\gamma-1)T(1)}{\sqrt{\omega \mathrm{Re}}}, \tag{46}$$

and

$$\bar{V}_2(z;\varepsilon) = \varepsilon a_0 + \varepsilon^2(a_4 + a_5 z + a_6 z^2) + \varepsilon^3(a_{11} + a_{12}z + a_{13}z^2 + a_{14}z^3 + a_{15}z^4), \tag{47a}$$

$$\bar{V}_3(z;\varepsilon) = \varepsilon^2 a_7 + \varepsilon^3(a_{16} + a_{17}z + a_{18}z^2). \tag{47b}$$

Note, in (45) the integrals are with respect to r rather than the boundary layer variable y. For χ_1 the transformation is trivial; for χ_μ the derivatives of the base flow variables produce powers of δ such that

$$\chi_\mu(r) = -\omega\delta^3\bar{\chi}_\mu(y), \qquad \text{with} \qquad \bar{\chi}_\mu(y) = \frac{1}{\omega - Uk}\left(\frac{1}{2\mathrm{Pr}}(T^2)_{yyy} + (TU_y^2)_y + \frac{kT}{\omega - Uk}(U_y T)_{yy}\right) \tag{48}$$

as shown later in (56b), where we have also chosen to incorporate an ω in the definition of $\chi_\mu(r)$.

A comparison of (42) and (45) with the numerical LNSE for the same parameters as figs. 1–3 is given in fig. 4. Excellent agreement can be seen between the LNSE and composite solutions, suggesting that the composite solutions may be relied upon when mode shapes are required, rather than having the complication of three separate solutions, each with their own region of validity.

The range of Reynolds number for which the asymptotic model is valid is investigated in fig. 5. The errors in the composite solutions for both $\tilde{p}$ and $\tilde{v}$ become significant when $\mathrm{Re} \lesssim 10^4$. This is partly due to

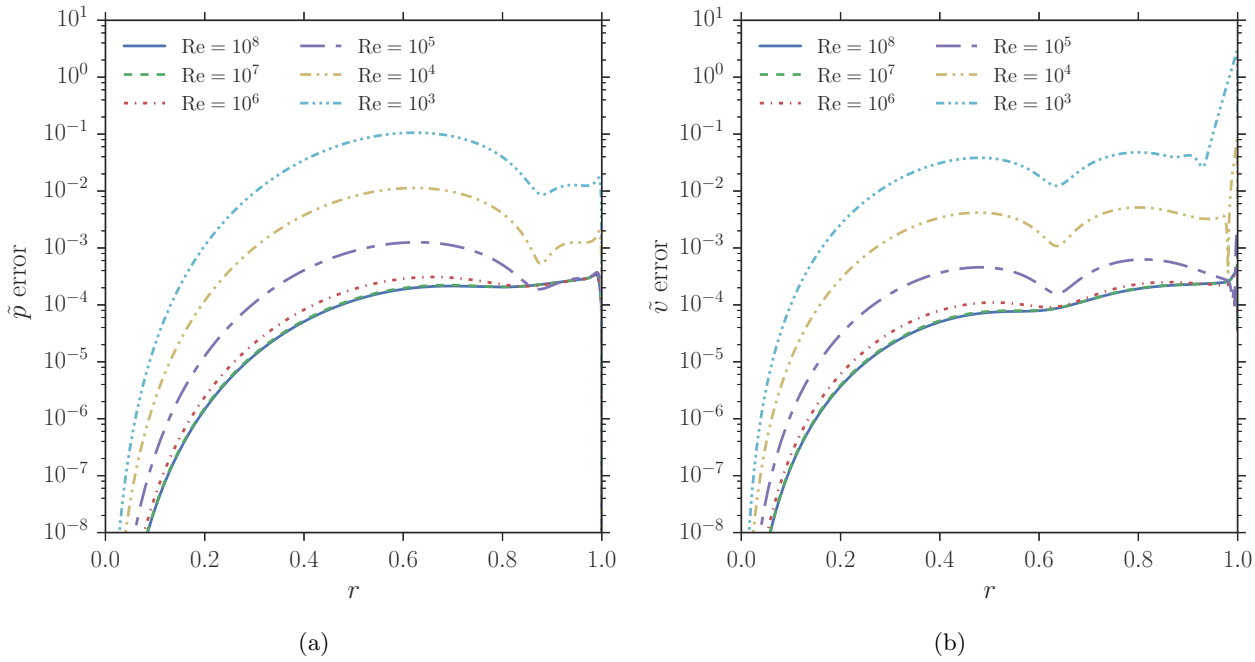

Figure 5. The error across the r domain of the composite solutions for (a) $\tilde{p}$ and (b) $\tilde{v}$ as the Reynolds number is decreased. We define error here as $|(\tilde{q}_n - \tilde{q}_c)/\text{mean}(\tilde{q}_n)|$, where $\tilde{q}_n$ is the LNSE numerical solution, and $\tilde{q}_c$ is the composite asymptotic solution. Parameters are $\omega = 15$, $k = 5 + 2i$, $m = 6$, $M = 0.5$, $\delta = 5 \times 10^{-3}$ for the tanh base flow.

the assumption that outside the boundary layer the acoustic solutions may be approximated by the inviscid uniform flow Bessel function solutions. Viscous effects are seen to alter the acoustic solutions further from the wall as Re is decreased, as expected [14, 25]. Figure 5b shows that the model predicts incorrect boundary layer behaviour for Re $\lesssim 10^4$, when the assumption of a weakly viscous main boundary layer breaks down. When Re $\gtrsim 10^5$ the composite solutions accurately reproduce the LNSE numerics across the full radius of the duct.

6. Effective impedance

The matched asymptotic expansions solutions for the acoustics derived in the previous sections, sections 2.B, 3 and 4, are used here to construct an effective impedance boundary condition. The effective impedance is defined as the impedance seen by the inviscid, uniform flow acoustics ($\tilde{p}_\text{u}$ and $\tilde{v}_\text{u}$ here) if they were continued out of their region of validity to the wall at $r = 1$, and is given by (10). This definition allows us to apply the resulting boundary condition to an inviscid, slipping, uniform flow, meaning the thin boundary layer does not need to be resolved numerically. The effective impedance differs from the boundary impedance Z due to viscothermal effects and refraction through the sheared boundary layer. We want to find Z_eff as a function of the boundary impedance Z.

We can use the information gleaned from matching the main boundary layer solution to the core flow in section 3.A, and from matching the main boundary layer solution to the viscous sublayer solution in section 4 to write the sublayer constants A_j, P_j in terms of the uniform flow constants p_∞ and v_∞:

$$\begin{aligned} &P_0 = p_\infty, \qquad P_2 = i\omega(\omega - Mk)I_0 v_\infty, \qquad A_0 = \frac{\omega}{\omega - Mk} v_\infty, \\ &A_2 = -i\omega^2 \frac{k^2 + m^2}{(\omega - Mk)^2} I_1 p_\infty - i\xi\omega(\gamma - 1)^2 \bar{I}_\mu \frac{\omega}{\omega - Mk} v_\infty, \end{aligned} \tag{49}$$

where I_0, I_1 and $\bar{I}_\mu$ are defined in (28).

At the boundary, the wall-normal velocity is

$$\tilde{v}_\text{s}(0) = A_0 + \varepsilon a_0 + \varepsilon^2(A_2 + a_4 + a_7) + \varepsilon^3(a_{11} + a_{16}),$$

We may split a_{11}, a_{16} and A_2 up into terms proportional to v_∞ and p_∞. Then we may write

$$\tilde{v}_\mathrm{s}(0) = p_\infty \left(\varepsilon^2 \bar{R}_1 + \varepsilon^3 \bar{S}_1\right) + \frac{\omega}{\omega - Mk} v_\infty \left(1 + \varepsilon \bar{R}_2 + \varepsilon^2 \bar{S}_2 + \varepsilon^3 \bar{S}_3\right), \tag{50}$$

where

$$\bar{R}_1 = -i\omega^2 \frac{k^2+m^2}{(\omega - Mk)^2} I_1, \tag{51a}$$

$$\bar{R}_2 = -\frac{kU'(0)}{\omega\eta}, \tag{51b}$$

$$\bar{S}_1 = i\omega \frac{k^2+m^2}{(\omega - Mk)^2} \frac{kU'(0)}{\eta} I_1 - i(\gamma-1)(k^2+m^2)\frac{T(0)}{\eta} - \frac{i(\gamma-1)\omega^2}{\sigma\eta}, \tag{51c}$$

$$\bar{S}_2 = -i\xi\omega(\gamma-1)^2 \bar{I}_\mu + \frac{\sigma}{1+\sigma}\frac{2U'(0)^2}{\eta^2 T(0)} - \frac{5k^2 U'(0)^2}{4\omega^2\eta^2}, \tag{51d}$$

$$\begin{aligned}\bar{S}_3 = {} & i\xi(\gamma-1)^2 \frac{kU'(0)}{\eta}\bar{I}_\mu - \frac{13k^2U'(0)U''(0)}{8\omega^2\eta^3} - \frac{kU'''(0)}{\omega\eta^3} - \frac{T'''(0)}{\sigma^3\eta^3 T(0)} - \frac{151k^3U'(0)^3}{32\omega^3\eta^3} \\ & + \frac{(7\sigma+3)}{(1+\sigma)^2}\frac{kU'(0)^3}{2\omega\eta^3 T(0)} + \frac{2(\sigma^3+\sigma^2-2\sigma-1)}{\sigma(1+\sigma)^2}\frac{U'(0)T''(0)}{\omega\eta^3 T(0)} - \frac{(2\sigma^2+4\sigma+1)}{(1+\sigma)^2}\frac{kU'(0)T''(0)}{\omega\eta^3 T(0)}.\end{aligned} \tag{51e}$$

Similarly, we may write $\tilde{p}_\mathrm{s}$ at $z = 0$:

$$\tilde{p}_\mathrm{s}(0) = p_\infty + \varepsilon^2 i\omega(\omega - Mk) I_0 v_\infty. \tag{52}$$

Then, we use the definition of the boundary impedance, $Z = \tilde{p}_\mathrm{s}(0)/\tilde{v}_\mathrm{s}(0)$, with $\tilde{p}_\mathrm{s}(0)$ and $\tilde{v}_\mathrm{s}(0)$ defined in (50) and (52), and divide top and bottom of the ratio by v_∞ to introduce the effective impedance $Z_\mathrm{eff} = p_\infty/v_\infty$:

$$Z = \frac{Z_\mathrm{eff} + \varepsilon^2 i\omega(\omega - Mk) I_0}{\frac{\omega}{\omega - Mk}\left(1 + \varepsilon\bar{R}_2 + \varepsilon^2\bar{S}_2 + \varepsilon^3\bar{S}_3\right) + Z_\mathrm{eff}\left(\varepsilon^2\bar{R}_1 + \varepsilon^3\bar{S}_1\right)}. \tag{53}$$

Rearranging, and writing in terms of r and primitive variables, then gives us our effective impedance in terms of the boundary impedance Z,

$$Z_\mathrm{eff} = \frac{\omega}{\omega - Mk}\frac{Z + \frac{(\gamma-1)T(1)}{\sqrt{i\omega\mathrm{Re}}}\frac{kU_r(1)}{\omega}Z - \frac{i}{\omega}(\omega - Mk)^2\delta I_0 + (S_2 + S_3)Z}{1 + i(k^2+m^2)\frac{\omega Z}{(\omega - Mk)^2}\delta I_1 + S_1 Z} + \mathcal{O}(\delta^2), \tag{54}$$

where

$$S_1 = \frac{(\gamma-1)T(1)}{\sqrt{i\omega\mathrm{Re}}}\left(\frac{k^2+m^2}{(\omega-Mk)^2} ikU_r(1)\delta I_1 + \frac{i\omega}{\sigma}(\gamma-1) + \frac{i}{\omega\rho(1)}(k^2+m^2)\right), \tag{55a}$$

$$S_2 = \left(\frac{(\gamma-1)T(1)}{\sqrt{i\omega\mathrm{Re}}}\right)^2\left(\frac{1}{T(1)^2}\frac{I_\mu}{\delta^2} + \frac{\sigma}{1+\sigma}\frac{2U_r(1)^2}{T(1)} - \frac{5k^2}{4\omega^2}U_r(1)^2\right), \tag{55b}$$

$$\begin{aligned}S_3 = {} & \left(\frac{(\gamma-1)T(1)}{\sqrt{i\omega\mathrm{Re}}}\right)^3\left(\frac{kU_r(1)}{\omega T(1)}\frac{I_\mu}{\delta^2} + \frac{13k^2}{8\omega^2}U_r(1)U_{rr}(1) + \frac{k}{\omega}U_{rrr}(1) + \frac{T_{rrr}(1)}{\sigma^3 T(1)}\right. \\ & + \frac{151k^3}{32\omega^3}U_r(1)^3 - \frac{(7\sigma+3)}{(1+\sigma)^2}\frac{kU_r(1)^3}{2\omega T(1)} - \frac{(\sigma^3+\sigma^2-2\sigma-1)}{\sigma(1+\sigma)^2}\frac{2U_r(1)T_{rr}(1)}{\omega T(1)} \\ & \left. + \frac{(2\sigma^2+4\sigma+1)}{(1+\sigma)^2}\frac{kU_r(1)T_{rr}(1)}{\omega T(1)}\right),\end{aligned} \tag{55c}$$

and

$$\delta I_0 = \int_0^1 1 - \frac{\rho(r)(\omega - U(r)k)^2}{(\omega - Mk)^2}\mathrm{d}r, \qquad \delta I_1 = \int_0^1 1 - \frac{(\omega - Mk)^2}{\rho(r)(\omega - U(r)k)^2}\mathrm{d}r. \tag{56a}$$

$$\frac{I_\mu}{\delta^2} = \int_0^1 \frac{\chi_\mu}{\delta^3}\mathrm{d}r, \qquad \frac{\chi_\mu}{\delta^3} = \frac{-\omega}{\omega - Uk}\left(\frac{1}{2\mathrm{Pr}}(T^2)_{rrr} + (TU_r^2)_r + \frac{kT}{\omega - Uk}(U_r T)_{rr}\right), \tag{56b}$$

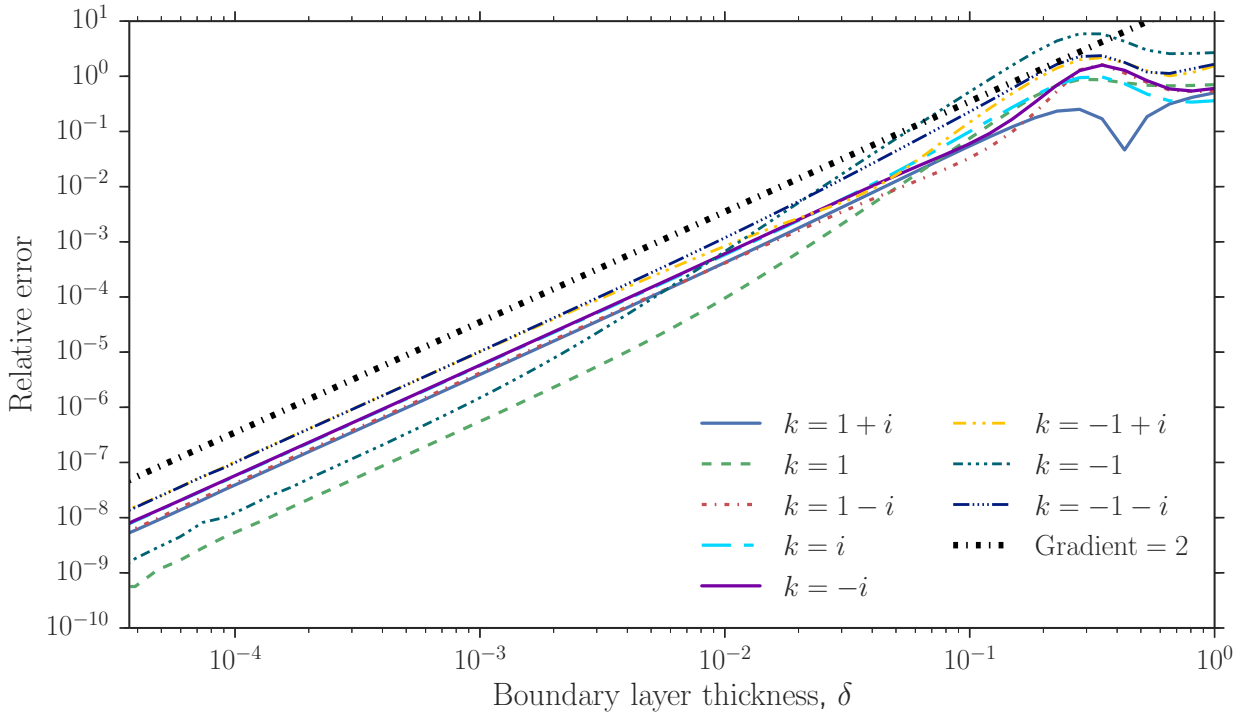

Figure 6. The error in the predicted impedance $Z_{\text{eff}}(Z)$ from (54) relative to the analytical value found using (10). The relative error is defined as $|Z_{\text{eff}}(Z_n)/Z_u - 1|$, where $Z_n = \tilde{p}_n(1)/\tilde{v}_n(1)$ is the true impedance calculated from the numerical LNSE solution of (4) and $Z_u = \tilde{p}_u(1)/\tilde{v}_u(1)$ is the uniform impedance, (10), calculated from the uniform flow solutions (9). Parameters are $\omega = 5$, $m = 0$, $M = 0.5$, $\text{Re} = 1/\delta^3$, with the hyperbolic base flow (41).

where as mentioned in section 5.B we have incorporated a power of ω in the definition of χ_μ compared to that of $\bar{\chi}_\mu$. Equation (54) is one of the main results of this paper, and provides an effective impedance Z_{eff} to be applied to inviscid plug flow acoustics that accounts for the effect of the viscous boundary layer over a lining. The plot of the relative error between the asymptotic expression for Z_{eff} in (54) and the exact expression (10), fig. 6, shows that (54) is correct to the stated order of accuracy.

7. Results

To find duct modes of our new effective impedance boundary condition (54), we must first choose a model for the acoustic liner impedance. Here, we use a mass–spring–damper boundary with a mass d, spring constant b and damping coefficient R, which gives the impedance

$$Z(\omega) = i\omega d - ib/\omega + R, \tag{57}$$

where ω is allowed to be complex [26, 27]. The dispersion relation to be satisfied is then

$$Z_{\text{eff}}(Z) = \frac{\tilde{p}_u(1)}{\tilde{v}_u(1)} = (\omega - Mk)\frac{J_m(\alpha)}{i\alpha J_m'(\alpha)}, \tag{58}$$

to find values of k (or ω) when ω (or k) is specified (given m). This relation comes from our definition of the effective impedance as that impedance seen by the uniform-flow inviscid solution at the wall. The function $Z_{\text{eff}}(Z)$ is the asymptotic effective impedance found using (54) with the boundary impedance Z from (57) as input. Examples of existing effective impedance boundary conditions are the Myers boundary condition [28, 29], which may be written

$$Z_{\text{eff}} = \frac{\omega}{\omega - Mk}Z, \tag{59}$$

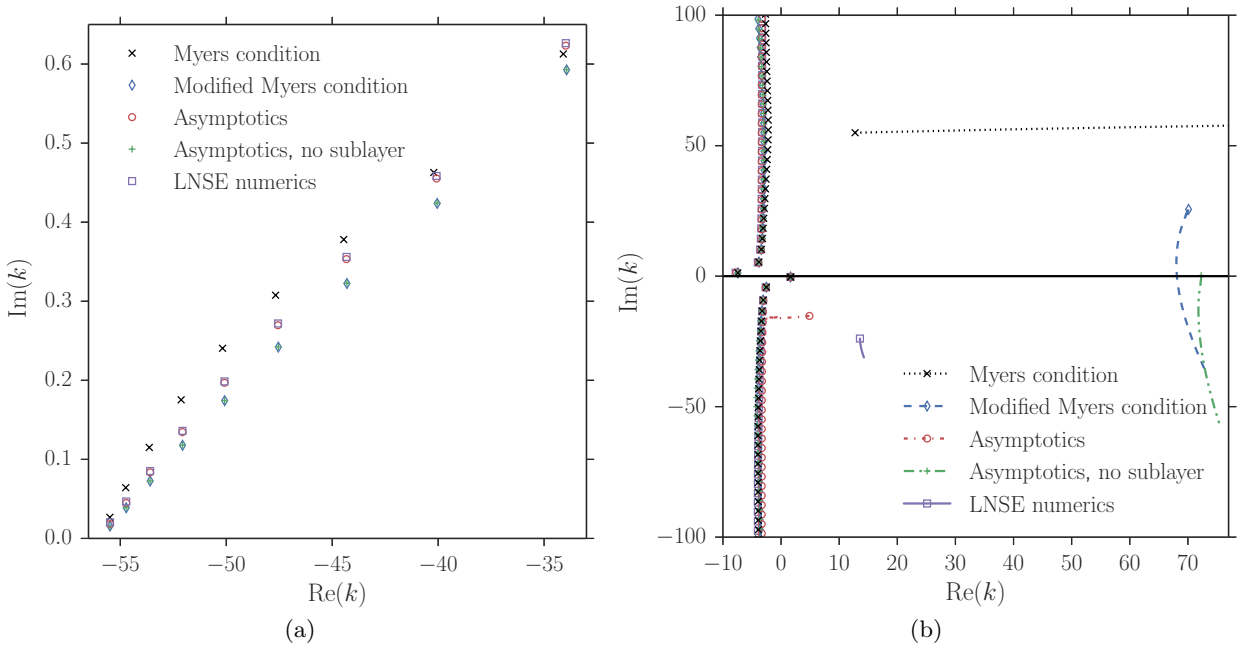

Figure 7. Duct modes in the complex k-plane of the Myers boundary condition (59), the modified Myers boundary condition (60), the new two-deck asymptotic condition (54), the one-deck (no sublayer) simplification of the new condition (61) and numerical solution of the LNSE (4). (a) shows upstream cuton modes for $\omega = 28$, $m = 0$, $M = 0.5$, $\delta = 2 \times 10^{-3}$, and $\mathrm{Re} = 5 \times 10^6$; (b) shows cutoff modes and one surface wave mode for each model, with $\omega = 5$, $m = 0$, $M = 0.5$, $\delta = 2 \times 10^{-3}$, and $\mathrm{Re} = 2.5 \times 10^5$. Mode tracks follow the surface wave modes as $\mathbb{I}\mathrm{m}(\omega)$ is reduced from zero to $\mathbb{I}\mathrm{m}(\omega) \approx -8$ with $\mathbb{R}\mathrm{e}(\omega) = 5$ held fixed. In both (a) and (b), the boundary impedance is a mass–spring–damper (57) with mass $d = 0.15$, spring constant $b = 1.15$ and damping $R = 3$. The base flow (41) is used.

and its first order correction [10] (called the modified Myers condition here),

$$Z_{\mathrm{eff}} = \frac{\omega}{\omega - Mk} \frac{Z - \frac{i}{\omega}(\omega - Mk)^2 \delta I_0}{1 + i(k^2 + m^2)\frac{\omega Z}{(\omega - Mk)^2}\delta I_1}, \tag{60}$$

where δI_0 and δI_1 are as defined in (56). We will compare the new boundary condition (54) against these existing conditions, as well as against numerical solutions of the LNSE. As a way to test the importance of including the viscous sublayer in our asymptotic model, we will also compute results using the boundary condition

$$Z_{\mathrm{eff}} = \frac{\omega}{\omega - Mk} \frac{Z - \frac{i}{\omega}(\omega - Mk)^2 \delta I_0 + \frac{(\gamma-1)^2}{i\omega \mathrm{Re}} \frac{I_\mu}{\delta^2}}{1 + i(k^2 + m^2)\frac{\omega Z}{(\omega - Mk)^2}\delta I_1}, \tag{61}$$

which is the effective impedance that would be obtained if the main boundary layer solutions were used to compute the boundary impedance, $\tilde{p}_{\mathrm{m}}(0)/\tilde{v}_{\mathrm{m}}(0) = Z$ (arguments in terms of y), rather than the viscous sublayer solutions. (That is, the Z_{eff} of a one-deck weakly viscous boundary layer above a lining.)

A. Wavenumber spectra

In fig. 7 a frequency is specified and (58) is solved to find allowed values of the axial wavenumber k. Figure 7a shows the upstream propagating cuton modes for the new asymptotic model with, (54), and without, (61), the viscous sublayer, the Myers condition (59), the modified Myers boundary condition (60), and the viscous numerics (4). The damping of these propagating modes is predicted poorly by the Myers condition, which can lead to large errors in sound attenuation computations (up to 14dB [24]) due to the effect of the nonzero boundary layer thickness. The new boundary condition (54) is shown to predict the damping of these modes well, and certainly better than the inviscid modified Myers condition, indicating that viscosity can play an important role in attenuation predictions. Figure 7a also shows the importance of calculating the contribution

to the sound attenuation of the viscous sublayer: the one-deck weakly viscous model (61) predicts cuton modes that are only marginally different to those of the inviscid modified Myers condition.

Figure 7b shows a surface wave mode for each model (those modes which exist only close to the lining). The two existing inviscid boundary conditions have surface wave modes in the upper half k-plane, while the new boundary condition predicts a surface wave mode in the lower half k-plane, close to the real LNSE mode. The change in sign of $\mathbb{I}\mathrm{m}(k)$ between the inviscid and viscous surface modes has important ramifications for the flow stability. By plotting Briggs–Bers trajectories of the surface wave modes (shown in the same figure) where $\mathbb{R}\mathrm{e}(\omega) = 5$ is held fixed and $\mathbb{I}\mathrm{m}(\omega)$ is reduced from zero, the stability may be investigated. Figure 7b shows the modified Myers surface mode crossing the real axis, indicating that the mode is convectively unstable. The surface modes of the new asymptotic boundary condition and the full LNSE are seen to remain in the lower half k-plane as $\mathbb{I}\mathrm{m}(\omega)$ is varied; thus the inviscid convective instability is stabilised by viscosity in the boundary layer. The surface mode of the one-deck model (61) is closer to the real axis than the modified Myers surface mode, but remains in the upper half plane; the plotted Briggs-Bers trajectory of the one-deck boundary condition mode, which crosses the real axis, therefore indicates that the convective instability is also present for this model. Thus, resolving the viscous sublayer has important ramifications for the stability of the boundary layer. The Briggs-Bers stability criteria cannot be applied for the Myers condition [30].

The effective impedance boundary condition (54) may be validated against the experimental prediction by Marx et al. [13] of the axial wavenumber of a hydrodynamic instability mode. The experimental work was performed in a rectangular duct with a fully turbulent mean flow, so we can expect only rough agreement between our asymptotics and the experiment. We approximate the boundary layer profile by the hyperbolic profiles in (41) with $\delta = 0.1$, as the asymptotic boundary condition needs the third derivative of the mean flow profile. The experimental mode [13] is $k_{\mathrm{exp}} = 1.3 + 0.3i$ (after conjugating to account for our $\exp\{i\omega t\}$ sign choice). An LNSE numerical mode is found at $k_n = 0.74 + 0.22i$ unstable via a Briggs–Bers analysis, fig. 8, which is shown to be very well approximated by the asymptotic boundary condition (table 2). Given the rough approximations made in replicating the experimental setup of Marx et al. [13], an error of 45% is still very acceptable—the numerical study of Marx and Aurégan [31] find an error of less than 30% in their replication of the same hydrodynamic mode, but their model uses a fully turbulent boundary layer profile and is solved numerically.

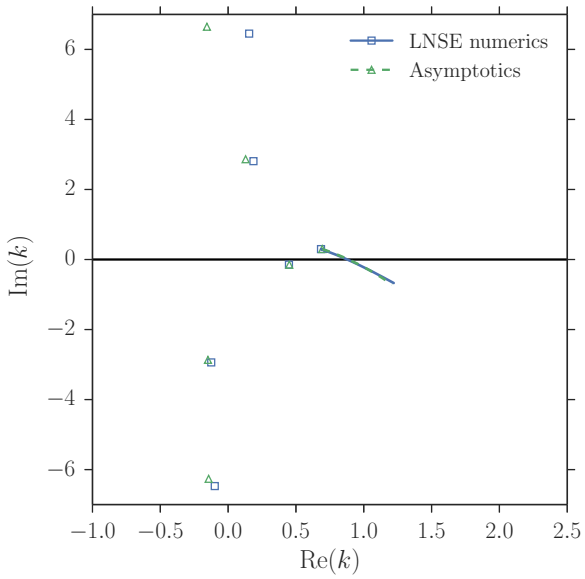

Figure 8. Modes of the LNSE and asymptotic boundary condition (at markers) and their Briggs–Bers contours as the imaginary part of the frequency is reduced from zero (lines). The parameters are taken from the experimental study of Marx et al. [13] and converted to the nondimensionalisation and definitions used here: $\mathbb{R}\mathrm{e}\,(\omega) = 0.188$, $-0.2 \leq \mathbb{I}\mathrm{m}\,(\omega) \leq 0$, $m = 0$, $M = 0.3194$, $\delta = 0.1$, $\mathrm{Re} = 2.3 \times 10^5$ (where we recalculate Re using our definition, (7)). The impedance is found using $Z = -i/Q \cot(A\omega^* - i\epsilon/2)$, where $Q = 0.8$, $A = 0.00025$, $\epsilon = 0.37$, $\omega^* = 1060 \times (2\pi)$. The boundary layer profile is approximated by the hyperbolic profiles of (41).

	k
LNSE	0.73976038 + 0.21997134i
Asymptotics	0.69409557 + 0.29937782i
Experimental [13]	1.3+0.3i

Table 2. Mode values at markers in fig. 8 and the experimental value from the Marx et al. [13] study after conjugation due to our sign choice in the $\exp\{i\omega t\}$ acoustic perturbations.

B. Temporal stability

In contrast with the previous section, here we pick a real k and solve (58) for $\omega(k)$. The temporal growth rate of such a mode is given by $-\mathbb{I}\mathrm{m}(\omega)$. In fig. 9 the temporal stability of complex-frequency duct modes is investigated as k, real, is varied for the LNSE and the asymptotic boundary condition (54). Several stable modes can be seen in the upper right of the plot — these are representative of other stable modes outside of the plotted domain. The important modes for stability are those below the horizontal axis, as these are unstable. The unstable LNSE mode has a growth rate that increases to a maximum value (a characteristic growth rate of instability) before decreasing and finally restabilising for large, finite k. The unstable root for the asymptotic solution follows a qualitatively similar path until the point labelled 'B' on fig. 9. To the left of 'B', the asymptotic mode has a bounded growth rate. This suggests that the boundary condition (54) retains the regularisation – obtained in previous inviscid modified Myers boundary conditions by including a finite-thickness layer of shear – of the Myers condition vortex sheet instability (inherent in approximations ignoring $\mathcal{O}(\delta)$ terms). To the right of 'B' the asymptotic solution supports no unstable modes.

Figure 10 displays a diagnosis of the point 'B'. As the asymptotic solution approaches the point 'B' from the left, the value of $|\omega - U(r)k|$ tends to zero, see fig. 10a. This is precisely the inviscid critical layer r_c, for which $\omega/k = U(r_c)$ and the perturbations are perfectly convected with the flow [32]. Close to the critical layer, the integrals I_μ and I_1 blow up (see fig. 10b), causing unphysical discontinuities in the acoustic solutions. Figure 11a shows the results of increasing the resolution of the numerical integration used to find these solutions. With higher numerical resolution of the integrals, the unstable asymptotic mode can be tracked closer to the real axis and stability, and closer to the critical layer. This adds weight to our conclusion that the unstable mode disappears into the critical layer at the point B.

It is known that changing the boundary layer profile can change the stability properties of the acoustics [9]. Figure 12 shows that the new boundary condition is able to capture the altered temporal stability of the LNSE system when the boundary layer profile is changed from the hyperbolic forms in (41) to a constant-

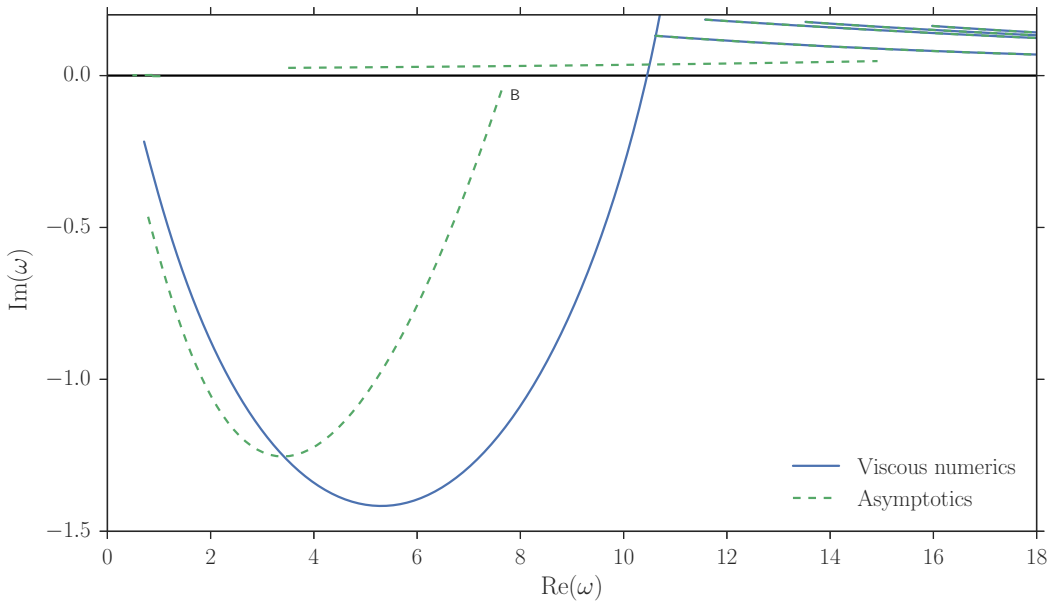

Figure 9. Modes in the ω plane as k, real, is increased, for LNSE numerics (solid) and the asymptotic solution (54) (dashed). The point labelled 'B' is where the regular unstable solution branch breaks down. Parameters are $m = 0$, $M = 0.5$, $\mathrm{Re} = 7\times10^6$, $\delta = 5 \times 10^{-3}$, with a mass–spring–damper impedance (57) with mass $d = 0.15$, spring constant $b = 1.15$ and damping $R = 3$. The base flow (41) is used.

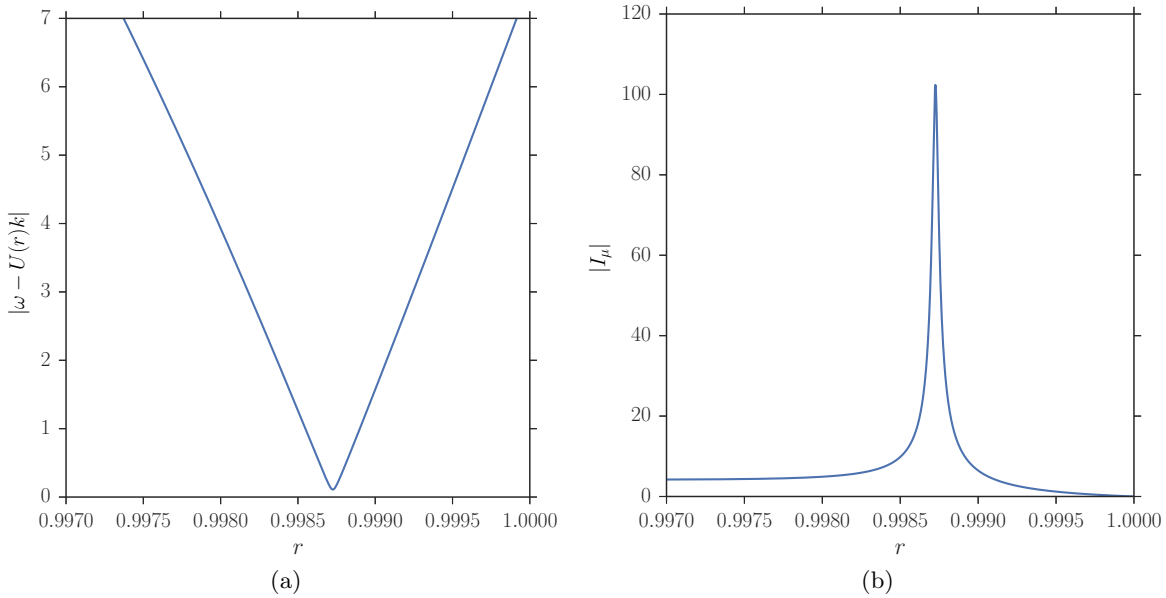

Figure 10. Evidence that the unstable solution in fig. 9 hits the critical layer at 'B'. (a) $|\omega - U(r)k|$, and (b) $|I_\mu|$, for $(\omega,\, k) = (7.51 - 0.11i,\, 60.21)$, and for other parameters as in fig. 9

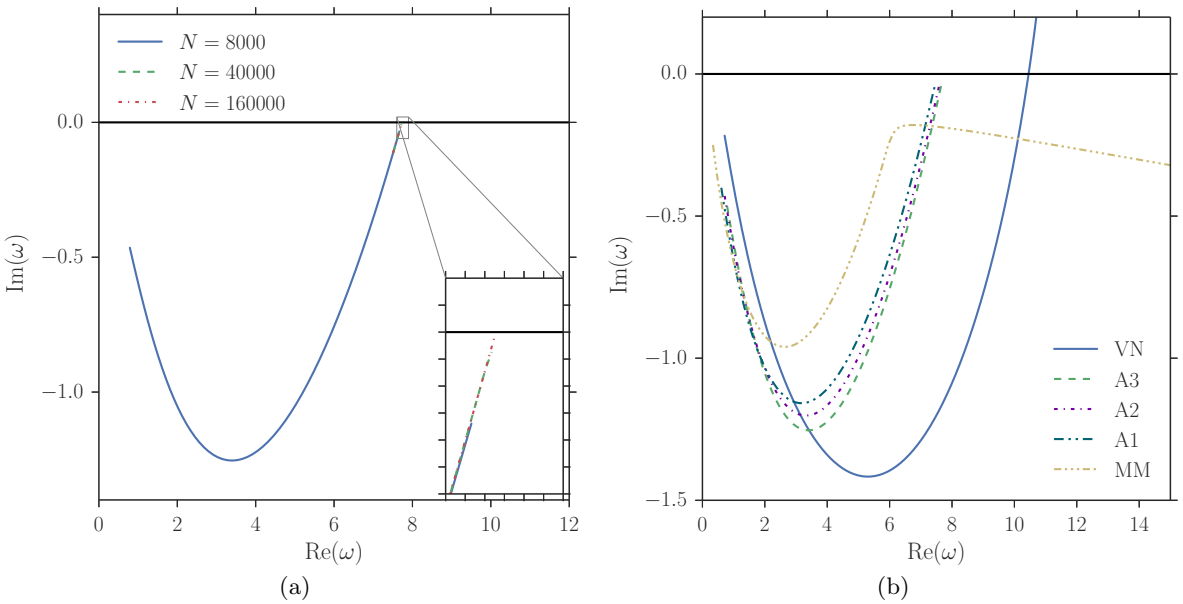

Figure 11. The behaviour of the unstable root in the ω-plane as k, real, is increased. (a) Results for the new asymptotic boundary condition (54) for three different discretisations, $N = 8000$, $N = 40000$, $N = 160000$. As the number of computational grid points is increased, the model is able to get closer to the inviscid critical layer $\omega - U(r_c)k = 0$, and the unstable mode is pushed closer to restabilisation, $\mathbb{I}\mathrm{m}(\omega) = 0$, before the solution breaks down. (b) Legend labels denote the viscous LNSE numerics (VN), the new asymptotic boundary condition (54) at $\mathcal{O}(\delta_{\mathrm{ac}}^3)$ (A3), at $\mathcal{O}(\delta_{\mathrm{ac}}^2)$ (A2), and at $\mathcal{O}(\delta_{\mathrm{ac}})$ (A1), and the modified Myers condition (60) (MM). For both (a) and (b) all parameters as in fig. 9.

then-linear mean flow with a constant base temperature. For the linear boundary layer profile, the unstable mode of the LNSE does not restabilise within the plotted domain, and the asymptotic model is able to capture this behaviour without interacting with the inviscid critical layer (as happens in the case of the tanh base flow profile). Thus, the new boundary condition is robust to changes in the parallel mean flow and the base temperature profile.

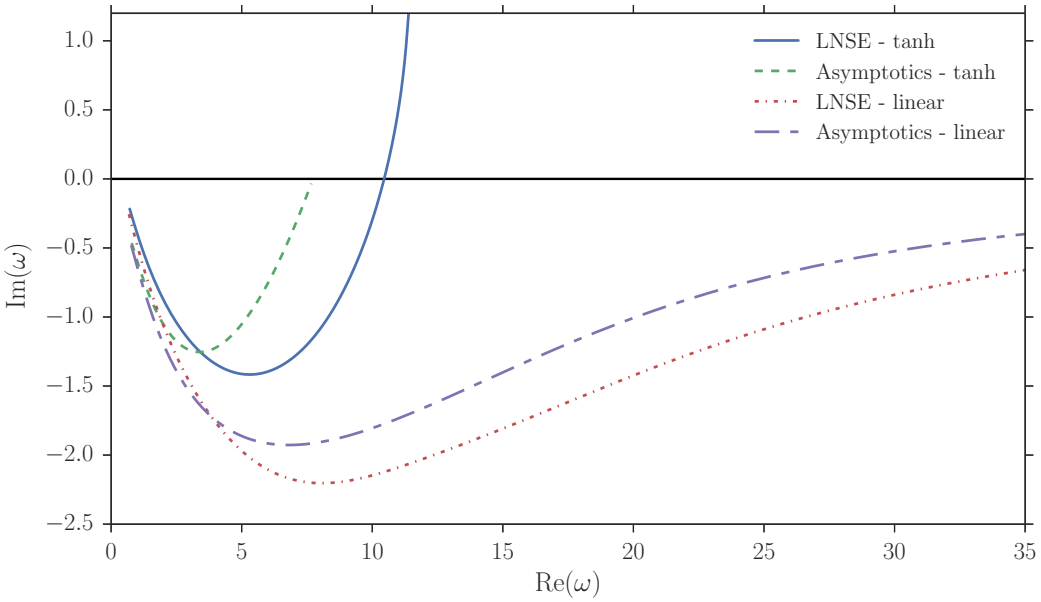

Figure 12. The behaviour of the unstable mode in the ω-plane as k, real, is increased, for the LNSE numerics and the asympotic boundary condition. Two boundary layer profiles are used: the hyperbolic base flow profiles of (41) (tanh) and a constant-then-linear mean flow with a constant base temperature (linear). Parameters are $m = 0$, $M = 0.5$, $\mathrm{Re} = 7 \times 10^6$, $\delta = 5 \times 10^{-3}$, with a mass–spring–damper impedance (57) with mass $d = 0.15$, spring constant $b = 1.15$ and damping $R = 3$.

8. Suggestion of a time-domain formulation

In order to write down a simple time-domain formulation of the new asymptotic frequency-domain boundary condition (54), we choose to neglect high-order viscous terms that do not affect the qualitative behaviour of the boundary condition too acutely. Using the definition of the acoustic boundary layer thickness δ_{ac} from (46), we see that the S_j terms of (54), defined in (55), satisfy

$$S_j \sim \delta_{\mathrm{ac}}^j. \tag{62}$$

Thus, retaining all three S_j terms means working to $\mathcal{O}(\delta_{\mathrm{ac}}^3)$; neglecting only S_3 means working to $\mathcal{O}(\delta_{\mathrm{ac}}^2)$; and neglecting both S_2 and S_3 means working to $\mathcal{O}(\delta_{\mathrm{ac}})$. In all cases we retain the $\mathcal{O}(\delta)$ inviscid terms that account for the finite region of shear. Figure 11b shows the temporal stability plots for the three choices outlined above. Qualitatively, the behaviour of the $\mathcal{O}(\delta_{\mathrm{ac}})$ form is the same as that of the $\mathcal{O}(\delta_{\mathrm{ac}}^3)$ form. We choose, then, to forego the $\mathcal{O}(\delta_{\mathrm{ac}}^3)$ in (54) in order to find the simplest time-domain formulation possible. (It transpires that the $\mathcal{O}(\delta_{\mathrm{ac}}^2)$ terms to not add much complexity to the final formulation, so they are kept here for completeness.)

We choose a constant-then-linear mean flow profile with boundary layer thickness δ,

$$U(r) = \begin{cases} U_0 \dfrac{(1-r)}{\delta}, & 1-\delta \le r \le 1, \\ U_0, & 0 \le r \le 1-\delta, \end{cases} \tag{63}$$

and a constant mean temperature and density, $T(r) = T_0$ and $\rho(r) = \rho_0$, respectively. This allows the boundary layer integrals I_j to be performed analytically:

$$\delta I_0(\omega - U_0 k)^2 = \frac{2}{3}\delta U_0^2 k^2 - \delta U_0 k\omega, \qquad \delta I_1 = \frac{\delta U_0 k}{\omega}, \qquad \frac{I_\mu}{\delta^2} = 0. \tag{64}$$

Rearranging the effective impedance boundary condition (54) using (63) and (64), and discarding the S_3 term as per the discussion in the previous paragraph, leads to

$$\left[\omega Z - \frac{U_0 k}{\delta\sqrt{\mathrm{Re}}}\frac{Z}{\sqrt{i\omega}} + i\delta\rho_0(U_0 k\omega - \frac{2}{3}U_0^2 k^2) + \omega Z S_2\right]\tilde{v}_{\mathrm{u}} = \left[(\omega - U_0 k) + i\delta U_0 k Z \frac{(k^2+m^2)}{\rho_0(\omega - U_0 k)} + (\omega - U_0 k) Z S_1\right]\tilde{p}_{\mathrm{u}}, \tag{65}$$

where the S_j terms simplify to

$$S_1 = \frac{1}{\sqrt{Re}}\left[\frac{(k^2+m^2)}{\rho_0(\omega-U_0k)^2}U_0^2k^2\frac{1}{i\omega\sqrt{i\omega}} + \frac{1}{\sigma T_0}\sqrt{i\omega} - \frac{(k^2+m^2)}{\rho_0}\frac{1}{i\omega\sqrt{i\omega}}\right], \tag{66a}$$

$$S_2 = \frac{1}{\delta^2\mathrm{Re}}\left[\frac{\sigma}{1+\sigma}\frac{2U_0^2}{T_0}\frac{1}{i\omega} - \frac{5}{4}\frac{U_0^2k^2}{\omega^2}\frac{1}{i\omega}\right]. \tag{66b}$$

To proceed, we follow Brambley and Gabard [19] by introducing a number of new variables, the interpretation of which we leave until later. First, we appeal to the fact that $\tilde{p}_\mathrm{u}$ satisfies the inviscid linearised Euler equations in a uniform flow to make the substitution $k\tilde{p}_\mathrm{u}/\rho_0(\omega-U_0k) = \tilde{u}_\mathrm{u}$. Then, we define $\tilde{v}_w = \tilde{p}_\mathrm{u}/Z$ and $\tilde{\nu} = \tilde{v}_\mathrm{u}/Z$, which arise when we divide (65) through by Z.

If in the frequency domain there exists a vector $\tilde{\mathbf{s}} = \tilde{\mathbf{u}}_\mathrm{u}/i\omega$, where $\tilde{\mathbf{u}}_\mathrm{u} = (\tilde{u}_\mathrm{u}, \tilde{v}_\mathrm{u}, \tilde{w}_\mathrm{u})$ is a vector of (the Fourier transform of) the acoustic velocity perturbations, then in the time domain

$$\frac{\partial \mathbf{s}'}{\partial t} = \mathbf{u}', \tag{67}$$

where a prime denotes an acoustic perturbation in the time domain. By (67) we may identify $\mathbf{s}' = (s_1', s_2', s_3')$ as the acoustic displacement vector in the coordinate directions (x, r, θ); it follows that $\tilde{\mathbf{s}}$ is the frequency-domain Fourier transform of $\mathbf{s}'$. To deal with the fractional powers of ω, we introduce the fractional time-derivative operator $\partial_t^{\frac{1}{2}}$ [see, e.g., 33]), which has the Fourier transform property

$$\mathcal{F}\{\mathbf{s}'\} = \tilde{\mathbf{s}} \qquad \Longrightarrow \qquad \mathcal{F}\left\{\partial_t^{\frac{1}{2}}\mathbf{s}'\right\} = \sqrt{i\omega}\tilde{\mathbf{s}}. \tag{68}$$

Using (67) and (68) and the definitions in the previous paragraph, (65) may be written in the time-domain as

$$\begin{aligned}\frac{\partial v'}{\partial t} = {}& \left(\frac{\partial}{\partial t} + \mathbf{U}_0\cdot\boldsymbol{\nabla}\right)v_w + \delta\mathbf{U}_0\cdot\left(\boldsymbol{\nabla}_\perp^2\mathbf{u}'\right) + \delta\rho_0\mathbf{U}_0\cdot\boldsymbol{\nabla}\left(\frac{\partial}{\partial t} + \frac{2}{3}\mathbf{U}_0\cdot\boldsymbol{\nabla}\right)\nu - \frac{1}{\delta\sqrt{\mathrm{Re}}}\mathbf{U}_0\cdot\boldsymbol{\nabla}\left(\partial_t^{\frac{1}{2}}s_2'\right)\\
&+ \frac{1}{\sqrt{\mathrm{Re}}}\left\{\left(\mathbf{U}_0\cdot\boldsymbol{\nabla}\right)\mathbf{U}_0\cdot\boldsymbol{\nabla}_\perp^2\left(\partial_t^{\frac{1}{2}}\mathbf{e}'\right) + \frac{1}{\sigma T_0}\left(\frac{\partial}{\partial t} + \mathbf{U}_0\cdot\boldsymbol{\nabla}\right)\left(\partial_t^{\frac{1}{2}}p'\right) + \frac{1}{\rho_0}\left(\frac{\partial}{\partial t} + \mathbf{U}_0\cdot\boldsymbol{\nabla}\right)\nabla_\perp^2\left(\partial_t^{\frac{1}{2}}\phi'\right)\right\}\\
&- \frac{1}{\delta^2\mathrm{Re}}\left\{\frac{\sigma}{1+\sigma}\frac{2}{T_0}|\mathbf{U}_0|^2v' + \frac{5}{4}\left(\mathbf{U}_0\cdot\boldsymbol{\nabla}\right)^2e_2'\right\},\end{aligned} \tag{69}$$

where $\nabla_\perp$ gives the gradient normal to the wall, and

$$\frac{\partial f'}{\partial t} = p', \qquad \frac{\partial \phi'}{\partial t} = f', \qquad \frac{\partial \mathbf{e}'}{\partial t} = \mathbf{s}', \tag{70}$$

and $\mathbf{s}'$ is defined in (67). The subscript on the s_j' and e_j' scalars refer to the jth component of the $\mathbf{s}'$ and $\mathbf{e}'$ vectors, respectively. Thus,

$$\frac{\partial e_2'}{\partial t} = s_2', \qquad \text{and} \qquad \frac{\partial s_2'}{\partial t} = v', \tag{71}$$

as v' is the second component of the time-domain acoustic velocity vector $\mathbf{u}'$. Note that these new variables $\mathbf{s}$, $\mathbf{e}$, ν, v_w and ϕ are only ever needed on the lining at $r = 1$.

The physical interpretation of v_w and ν (of which $\tilde{v}_w$ and $\tilde{\nu}$ are the Fourier transforms) is contained within the time domain boundary model [19]. If v_w is the wall-normal velocity response of the wall due to an acoustic pressure p' through the impedance model $\mathcal{B}(p')$, then ν is the response through the same impedance model forced by the normal fluid velocity, $\mathcal{B}(v')$. For the mass–spring–damper model (57) that we have employed in previous sections of this paper, v_w and ν satisfy

$$\frac{\partial v_w}{\partial t} = \frac{1}{d}\left[p' - b\psi - Rv_w\right], \qquad \frac{\partial \psi}{\partial t} = v_w, \tag{72a}$$

$$\frac{\partial \nu}{\partial t} = \frac{1}{d}\left[v' - b\zeta - R\nu\right], \qquad \frac{\partial \zeta}{\partial t} = \nu. \tag{72b}$$

The study of lossy waves in the time domain often leads to wave equations with fractional time derivatives [34, 35]. Therefore the appearance of the operator $\partial_t^{\frac{1}{2}}$ in (69) is expected, due to the inclusion of viscous and thermal dissipation. An implementation of the proposed time-domain formulation is left for future work, although it is hypothesised that a combination of the method used in Brambley and Gabard [19] and the Grünwal-Letnikov finite difference scheme for the non-integer order derivatives [see, e.g., 36] might be profitable.

9. Conclusion

In the current work we have assumed a mean flow with a high Reynolds number $\mathrm{Re} = U^*\ell^*/\nu^*$, a subsonic Mach number $0 < M = U^*/c^* < 1$, and a thin mean-flow boundary layer of thickness $\delta \sim \mathrm{Re}^{-1/3}$. This boundary layer is thicker than the laminar Blasius boundary layer thickness of $O(\mathrm{Re}^{-1/2})$, and is motivated by realistic aircraft engine flows and laboratory experiments investigating flows over acoustic linings. On top of this mean flow, sound of frequency Ω^* (with Helmholtz number $\omega = \Omega^*\ell^*/c^*$) is assumed, giving an acoustic boundary layer of thickness $(\omega\mathrm{Re})^{-1/2}$ which is thinner than the mean flow boundary layer. In doing so, we have not made any assumptions about the sound being high frequency, nor about the velocity or temperature profiles of the mean flow boundary layer, unlike previous works which have found such assumptions necessary in order to give analytic solutions; the only regime in which our asymptotic assumptions break down is the very low frequency limit for which the Helmholtz number $\omega \lesssim \mathrm{Re}^{-1/3}$. By solving separately for the acoustics in the three regions, being the outer inviscid uniform-flow region, the sheared mean-flow boundary layer, and the viscous acoustic sublayer, matching the solutions together yields an effective impedance boundary condition $Z_{\mathrm{eff}} = \tilde{p}_{\mathrm{u}}(1)/\tilde{v}_{\mathrm{u}}(1)$ (54). This effective impedance boundary condition can be applied to acoustics in slipping inviscid flow, and accounts for the effects of shear and viscosity within the boundary layer. It is anticipated this boundary condition could be used in frequency-domain numerics to avoid having to mesh finely and solve for the acoustics within the thin boundary layers at the walls. The new boundary condition appears to be valid for Reynolds numbers $\mathrm{Re} \gtrsim 10^4$, and is robust to changes in the parellel mean flow profile and base temperature profile.

While the use of three separate regions might seem unwieldy, should details of the acoustics within the boundary layer be necessary, the uniformly-valid composite expansions (42) and (45) may be used. These composite expansions give the correct asymptotic behaviour when evaluated in each of the three regions, and were shown to agree well with the full LNSE numerics.

Viscosity is known to play an important role within boundary layers over acoustic linings. This was demonstrated here in figs. 1–3 by the major effect of the viscous sublayer. Further, fig. 7 demonstrated that viscosity is necessary to accurately predict the attenuation of cuton upstream-propagating modes, which is an important parameter for the understanding of fan forward noise. Figure 11b suggests that shear effects dominate viscous effects within the mean flow boundary layer, while viscosity dominates within the viscous sublayer.

For the parameters used here, flow over an acoustic liner is unstable, as shown in figs. 7b and 9 for the full LNSE. The asymptotics derived here correctly reproduce this stability behaviour away from the critical layer. The authors have previously found that instability can be avoided altogether provided the Reynolds number is sufficiently low [18]. Near the critical layer the integrals become singular and the asymptotic solution breaks down (fig. 10). Inviscid solutions similarly break down at or near the critical layer, and this is often not limiting when used in practice, although if accurate details are required around the critical layer a full LNSE solutions is probably advisable with high resolution around the critical layer to avoid numerical inaccuracies.

Previous investigations of viscous impedance boundary conditions, and many inviscid boundary conditions, have avoided the time domain. Due to the good temporal stability behaviour of the boundary condition presented here, a time-domain formulation of (54) is proposed in section 8. Equation (69) is the first time-domain impedance boundary condition to incorporate viscothermal effects. Implementation of this boundary condition as part of a time-domain linearised Euler equations solver is beyond the scope of this paper, and would constitute interesting future work. The recent success of an inviscid time-domain implementation [19] gives hope that the formulation proposed here will prove useful.

The assumption here of a mean flow boundary layer wider than predicted by laminar Blasius theory might be due to a turbulent boundary layer and the effects of an eddy viscosity. A reformulation of the current work that includes a realistic eddy viscosity that is strong at the edge of the boundary layer and

weak very close to the wall would be a pertinent extension [31], as would inclusion of the effects of the eddies themselves on the acoustics. The effects of swirl on the acoustics in a duct, neglected here, are also known to be appreciable. Incorporating a swirling mean flow would lead to a frequency-domain boundary condition applicable in such situations, where the current standard is the classical and ill-posed inviscid Ingard–Myers boundary condition.

A. Determining the sublayer scaling

We imagine a thin acoustic sublayer, of thickness δ_{ac}, very close to the wall. We rescale into this sublayer from r-space via $r = 1 - \delta_{\mathrm{ac}} z$, where z is the sublayer variable. We posit that y (the mean-flow boundary layer variable) and z are related by $y = \varepsilon z$, with $\varepsilon \ll 1$ to be determined.

Inside the sublayer, viscous and inertial terms must balance in order for viscous boundary conditions to be satisfied at the wall. The relevant terms in the linearised Navier–Stokes axial momentum equation are

$$i\rho(\omega - Uk)\tilde{u} \qquad \text{and} \qquad \frac{\gamma - 1}{\mathrm{Re}}(T\tilde{u}_r)_r. \tag{A1}$$

We want these two terms to balance the leading order of the sublayer governing axial momentum equation. Close to the wall, the base flow variables may be expanded for small y as

$$U(y) \sim yU'(0) + \mathcal{O}(y^2), \qquad T(y) \sim T(0) + \mathcal{O}(y^2), \tag{A2}$$

where we have used the no slip and isothermal boundary conditions $U(0) = 0$, $T'(0) = 0$. Using (A2) in (A1) and asserting that the leading order must balance we find

$$i\omega\tilde{u} \sim \frac{(\gamma - 1)^2 T(0)^2}{\delta_{\mathrm{ac}}^2 \mathrm{Re}}\tilde{u}_{zz}, \tag{A3}$$

where we have written the r derivatives in terms of the sublayer variable z. The combination $(\gamma-1)^2T(0)^2$ is $\mathcal{O}(1)$: $(\gamma - 1) = 1/T_0$ is the reciprocal of the dimensionless centreline base temperature; the ratio $T(0)/T_0 \simeq 1.15$ for a compressible Blasius boundary layer. Thus we are left with

$$\omega\tilde{u} \sim \frac{1}{\delta_{\mathrm{ac}}^2 \mathrm{Re}}\tilde{u}_{zz}, \tag{A4}$$

from which we may identify $\delta_{\mathrm{ac}}^2 \sim 1/\omega\mathrm{Re}$. This is the classical acoustic boundary layer scaling. We know that $\varepsilon\delta \sim \delta_{\mathrm{ac}}$ from the relationships between r, y and z. We also know $\delta \sim 1/\mathrm{Re}^{1/3}$ from our choice of main boundary layer scaling. Thus, we may define

$$\frac{1}{\mathrm{Re}} = \xi\omega^3\varepsilon^6 \tag{A5}$$

or equivalently $\varepsilon = \sqrt{\delta/\omega}$. The $\mathcal{O}(1)$ quantity ξ is the same as in (12). Relative to the main boundary layer the sublayer scales as $\varepsilon \sim \mathrm{Re}^{-1/6}$, while relative to the duct radius it scales as $\varepsilon\delta \sim \mathrm{Re}^{-1/2}$ which is the Blasius boundary layer scaling.

B. Solving inside the sublayer

Here we show the details of the solution of the sublayer governing equations (33). Solving at leading order:

$$\tilde{v}_{0z} = 0 \qquad \implies \tilde{v}_0 = A_0, \tag{B1a}$$

$$\hat{u}_{0zz} - \eta^2\hat{u}_0 = \frac{iU'}{\omega}\eta^2\tilde{v}_0 \qquad \implies \hat{u}_0 = B_0\mathrm{e}^{-\eta z} + C_0\mathrm{e}^{\eta z} - \frac{iU'}{\omega}A_0, \tag{B1b}$$

$$\frac{1}{\mathrm{Pr}}\hat{T}_{0zz} - \eta^2\hat{T}_0 = 0 \qquad \implies \hat{T}_0 = D_0\mathrm{e}^{-\sigma\eta z} + E_0\mathrm{e}^{\sigma\eta z}, \tag{B1c}$$

$$\tilde{p}_{0z} = 0 \qquad \implies \tilde{p}_0 = P_0, \tag{B1d}$$

$$\tilde{w}_{0zz} - \eta^2\tilde{w}_0 = -\frac{m}{\omega}(\gamma - 1)T\eta^2\tilde{p}_0 \implies \tilde{w}_0 = G_0\mathrm{e}^{-\eta z} + H_0\mathrm{e}^{\eta z} + \frac{m}{\omega}(\gamma - 1)TP_0, \tag{B1e}$$

where A_j, P_j, B_j, C_j, D_j, E_j, G_j, and H_j are constants of integration. In the sublayer we want to satisfy no slip at the boundary $z = 0$ and match to the main boundary layer in the limit $z \to \infty$. Solutions that grow exponentially in z are therefore not allowed; $C_0 = E_0 = H_0 = 0$, and similarly at all orders. No slip and isothermal wall conditions give

$$B_0 = \frac{iU'}{\omega}A_0, \qquad D_0 = 0, \qquad G_0 = -\frac{m}{\omega}(\gamma-1)TP_0. \tag{B2}$$

At first order we find

$$\tilde{v}_1 = A_1 + a_0 \mathrm{e}^{-\eta z} + a_1 z, \tag{B3}$$

where

$$a_0 = \frac{ik}{\eta}B_0 = -\frac{kU'}{\omega\eta}A_0, \qquad a_1 = ikB_0 = -\frac{kU'}{\omega}A_0. \tag{B4}$$

Then,

$$\hat{u}_1 = b_0 + b_1 z + (B_1 + b_2 z + b_3 z^2)\mathrm{e}^{-\eta z}, \tag{B5}$$

$$\hat{T}_1 = D_1 \mathrm{e}^{-\sigma\eta z} + d_0 z + d_1 \mathrm{e}^{-\eta z}, \tag{B6}$$

where

$$b_0 = -\frac{iU'}{\omega}A_1, \qquad b_1 = -\frac{iU''}{\omega}A_0, \qquad b_2 = \frac{3}{4}\frac{ikU'^2}{\omega^2}A_0, \qquad b_3 = \frac{ikU'^2}{4\omega^2}\eta A_0,$$
$$d_0 = -\frac{iT''}{\omega}A_0, \qquad d_1 = \frac{\mathrm{Pr}}{1-\mathrm{Pr}}\frac{2iU'^2}{\omega\eta}A_0, \qquad D_1 = -d_1.$$

No slip forces $B_1 = -b_0$. The first order pressure contribution is $\tilde{p}_1 = P_1$. Higher orders of the azimuthal velocity $\tilde{w}$ are not required to calculate $\tilde{p}$ and $\tilde{v}$ to the desired order.

At second order,

$$\tilde{v}_2 = A_2 + a_2 z + a_3 z^2 + (a_4 + a_5 z + a_6 z^2)\mathrm{e}^{-\eta z} + a_7 \mathrm{e}^{-\sigma\eta z} \tag{B7}$$

where

$$a_2 = -ikb_0, \qquad a_3 = -\frac{kU''}{2\omega}A_0, \qquad a_4 = \Big(-\frac{5}{4}\frac{k^2U'^2}{\omega^2\eta^2} - \frac{\mathrm{Pr}}{1-\mathrm{Pr}}\frac{2U'^2}{\eta^2 T}\Big)A_0 + \frac{ik}{\eta}B_1),$$
$$a_5 = -\frac{5}{4}\frac{k^2U'^2}{\omega^2\eta}A_0, \qquad a_6 = -\frac{k^2U'^2}{4\omega^2}A_0, \qquad a_7 = \frac{\mathrm{Pr}}{1-\mathrm{Pr}}\frac{2U'^2}{\sigma\eta^2 T}A_0.$$

Then,

$$\hat{u}_2 = b_4 + b_5 z + b_6 z^2 + (B_2 + b_7 z + b_8 z^2 + b_9 z^3 + b_{10} z^4)\mathrm{e}^{-\eta z} + b_{11}\mathrm{e}^{-\sigma\eta z}, \tag{B8}$$

$$\hat{T}_2 = d_2 + d_3 z + d_4 z^2 + (d_5 + d_6 z + d_7 z^2)\mathrm{e}^{-\eta z} + (D_2 + d_8 z + d_9 z^2)\mathrm{e}^{-\sigma\eta z}, \tag{B9}$$

where

$$b_4 = \Big(-\frac{iU'T''}{\omega\eta^2 T} - \frac{iU'''}{\omega\eta^2}\Big)A_0 + k(\gamma-1)TP_0 - \frac{iU'}{\omega}A_2, \qquad b_5 = -\frac{iU''}{\omega}A_1,$$
$$b_6 = -\frac{iU'''}{2\omega}A_0, \qquad b_7 = \Big(\frac{41}{32}\frac{ik^2U'^3}{\omega^3\eta} + \frac{3}{8}\frac{ikU'U''}{\omega^2\eta}\Big)A_0 + \frac{3kU'}{4\omega}B_1,$$
$$b_8 = \Big(\frac{21}{32}\frac{ik^2U'^3}{\omega^3} + \frac{3}{8}\frac{ikU'U''}{\omega^2}\Big)A_0 + \frac{kU'\eta}{4\omega}B_1, \qquad b_9 = \Big(\frac{11}{48}\frac{ik^2U'^3}{\omega^3}\eta + \frac{ikU'U''}{12\omega^2}\eta + \frac{iU'T''}{6\omega T}\eta\Big)A_0,$$
$$b_{10} = \frac{ik^2U'^3}{32\omega^3}\eta^2 A_0, \qquad b_{11} = -\frac{\mathrm{Pr}}{1-\mathrm{Pr}}\frac{2iU'^3}{\omega\sigma\eta^2 T}A_0,$$

with no slip giving $B_2 = -(b_4 + b_{11})$; and

$$d_2 = \Big(-\frac{2iU'U''}{\omega\eta^2} - \frac{iT'''}{\mathrm{Pr}\omega\eta^2}\Big)A_0 + (\gamma-1)T\omega P_0, \qquad d_3 = -\frac{iT''}{\omega}A_1, \qquad d_4 = -\frac{iT'''}{2\omega}A_0,$$
$$d_5 = \frac{\mathrm{Pr}}{1-\mathrm{Pr}}\Big(\frac{5+3\mathrm{Pr}}{2(1-\mathrm{Pr})}\frac{ikU'^3}{\omega^2\eta^2} + \frac{4}{1-\mathrm{Pr}}\frac{iU'U''}{\omega\eta^2} - \frac{2}{1-\mathrm{Pr}}\frac{ikU'T''}{\omega^2\eta^2}\Big)A_0 + \frac{\mathrm{Pr}}{1-\mathrm{Pr}}\frac{2U'}{\eta}B_1,$$
$$d_6 = \frac{\mathrm{Pr}}{1-\mathrm{Pr}}\Big(\frac{5}{2}\frac{ikU'^3}{\omega^2\eta} - \frac{ikU'T''}{\omega^2\eta} + \frac{2iU'U''}{\omega\eta}\Big)A_0, \qquad d_7 = \frac{\mathrm{Pr}}{1-\mathrm{Pr}}\frac{ikU'^3}{2\omega^2}A_0,$$
$$d_8 = -\frac{\mathrm{Pr}}{1-\mathrm{Pr}}\frac{ikU'^3}{2\omega^2\eta}A_0, \qquad d_9 = -\frac{\mathrm{Pr}\sigma}{1-\mathrm{Pr}}\frac{ikU'^3}{2\omega^2}A_0,$$

with $D_2 = -(d_2 + d_5)$ from the boundary condition at $z = 0$. For the pressure we find $\tilde{p}_2 = P_2$.

At third order, we find

$$\tilde{v}_3 = A_3 + a_8 z + a_9 z^2 + a_{10} z^3 + (a_{11} + a_{12}z + a_{13}z^2 + a_{14}z^3 + a_{15}z^4)\mathrm{e}^{-\eta z} + (a_{16} + a_{17}z + a_{18}z^2)\mathrm{e}^{-\sigma\eta z}, \tag{B10}$$
$$\tilde{p}_3 = P_3 + \frac{i\omega^2}{(\gamma-1)T}A_0 z. \tag{B11}$$

The constants are defined by

$$a_8 = \Big(i\omega^2 - i(k^2+m^2)(\gamma-1)T\Big)P_0 + \Big(-\frac{T'''}{\eta^2\mathrm{Pr}T} - \frac{2U'U''}{\eta^2 T} - \frac{kT''U'}{\eta^2\omega T} - \frac{kU'''}{\eta^2\omega} + \omega\Big)A_0 - \frac{kU'}{\omega}A_2,$$
$$a_9 = -\frac{kU''}{2\omega}A_1, \qquad a_{10} = -\frac{kU'''}{6\omega}A_0,$$
$$a_{11} = -A_0U'\left(\frac{151k^3U'^2}{32\eta^3\omega^3} + \frac{13k^2U''}{8\eta^3\omega^2} + \frac{k\mathrm{Pr}\left((\mathrm{Pr}-3)T'' + 4U'^2\right)}{\eta^3(\mathrm{Pr}-1)^2T\omega} - \frac{2(\mathrm{Pr}-3)\mathrm{Pr}U''}{\eta^3(\mathrm{Pr}-1)^2T}\right)$$
$$+8i\eta(\mathrm{Pr}-1)\omega^2\left(B_1U'\left(5k^2(\mathrm{Pr}-1)T - \frac{\mathrm{Pr}}{4\eta^3(\mathrm{Pr}-1)^2T\omega}\right) + \frac{B_2k - (\gamma-1)m^2P_0T}{8\eta^2(\mathrm{Pr}-1)\omega^2}\right),$$
$$a_{12} = U'\left(\frac{k\left(A_0\mathrm{Pr}\left(6U'^2 - 4T''\right) + \frac{5iB_1k}{32\eta\omega^3}\right)}{4\eta^2(\mathrm{Pr}-1)T\omega} - \frac{151A_0k^3U'^2}{32\eta^2\omega^3} - \frac{13A_0k^2U''}{8\eta^2\omega^2} + \frac{2A_0\mathrm{Pr}U''}{\eta^2(\mathrm{Pr}-1)T}\right),$$
$$a_{13} = kU'\left(8\omega^2\left(\frac{A_0\left(-\mathrm{Pr}T'' + \mathrm{Pr}U'^2 + T''\right)}{16\eta(\mathrm{Pr}-1)T\omega^3} + \frac{iB_1k}{32\omega^3}\right) - \frac{55A_0k^2U'^2}{32\eta\omega^3} - \frac{5A_0kU''}{8\eta\omega^2}\right),$$
$$a_{14} = -\frac{A_0kU'}{48T\omega^3}\left(17k^2TU'^2 + 4kTU''\omega + 8T''\omega^2\right), \qquad a_{15} = -\frac{A_0\eta k^3U'^3}{32\omega^3},$$
$$a_{16} = -\frac{3A_0\eta^3kTU'^3\omega}{2(\mathrm{Pr}-1)} + \frac{iD_2\eta^5T\omega^3}{\sigma}, \qquad a_{17} = -\frac{\sigma}{1-\mathrm{Pr}}\frac{A_0kU'^3}{2\eta^2T\omega},$$
$$a_{18} = \frac{\mathrm{Pr}}{1-\mathrm{Pr}}\frac{A_0kU'^3}{2\eta T\omega}.$$

Acknowledgements

DK was supported by an EPSRC doctoral training grant. EJB is grateful for the support of a Royal Society University Research Fellowship. A preliminary version of some of this work was presented at the 22nd AIAA/CEAS Aeroacoustics Conference, Lyon, 2016, paper 2016-2976.

References

[1] E. J. Rice, "Propagation of Waves in an Acoustically Lined Duct with a Mean Flow," *NASA Special Publication*, vol. 207, pp. 345–355, 1969.

[2] S.-H. Ko, "Sound Attenuation in Lined Rectangular Ducts with Flow and Its Application to the Reduction of Aircraft Engine Noise," *Journal of the Acoustical Society of America*, vol. 50, pp. 1418–1432, 1971.
[3] D. H. Tack and R. F. Lambert, "Influence of Shear Flow on Sound Attenuation in a Lined Duct," *The Journal of the Acoustical Society of America*, vol. 38, no. 4, pp. 655–666, 1965.
[4] P. Mungur and G. M. L. Gladwell, "Acoustic wave propagation in a sheared fluid contained in a duct," *Journal of Sound and Vibration*, vol. 9, no. 1, pp. 28–48, 1969.
[5] S.-H. Ko, "Sound attenuation in acoustically lined circular ducts in the presence of uniform flow and shear flow," *Journal of Sound and Vibration*, vol. 22, no. 2, pp. 193–210, 1972.
[6] Y. Renou and Y. Aurégan, "Failure of the Ingard-Myers boundary condition for a lined duct: An experimental investigation," *Journal of the Acoustical Society of America*, vol. 130, no. 1, pp. 52–60, 2011.
[7] M. O. Burak, M. Billson, L.-E. Eriksson, and S. Baralon, "Validation of a Time- and Frequency-Domain Grazing Flow Acoustic Liner Model," *AIAA Journal*, vol. 47, no. 8, pp. 1841–1848, 2009.
[8] S. W. Rienstra, "A Classification of Duct Modes Based on Surface Waves," *Wave Motion*, vol. 37, no. 2, pp. 119–135, 2003.
[9] E. J. Brambley, "Surface modes in sheared boundary layers over impedance linings," *Journal of Sound and Vibration*, vol. 332, pp. 3750–3767, 2013.
[10] ——, "Well-posed boundary condition for acoustic liners in straight ducts with flow," *AIAA Journal*, vol. 49, no. 6, pp. 1272–1282, 2011.
[11] S. W. Rienstra and M. Darau, "Boundary-layer thickness effects of the hydrodynamic instability along an impedance wall," *Journal of Fluid Mechanics*, vol. 671, pp. 559–573, 2011.
[12] Y. Aurégan and M. Leroux, "Experimental evidence of an instability over an impedance wall in a duct with flow," *Journal of Sound and Vibration*, vol. 317, pp. 432–439, 2008.
[13] D. Marx, Y. Aurégan, H. Bailliet, and J.-C. Valiére, "PIV and LDV evidence of hydrodynamic instability over a liner in a duct with flow," *Journal of Sound and Vibration*, vol. 329, pp. 3798–3812, 2010.
[14] D. Khamis and E. J. Brambley, "The Effective Impedance of a Finite-Thickness Viscothermal Boundary Layer Over an Acoustic Lining," 2015, aIAA Paper 2015-2229.
[15] A. H. Nayfeh, "Effect of the acoustic boundary layer on the wave propagation in ducts," *Journal of the Acoustical Society of America*, vol. 54, pp. 1737–1742, 1973.
[16] Y. Aurégan, R. Starobinski, and V. Pagneux, "Influence of grazing flow and dissipation effects on the acoustic boundary conditions at a lined wall," *The Journal of the Acoustical Society of America*, vol. 109, no. 1, pp. 59–64, 2001.
[17] E. J. Brambley, "Acoustic implications of a thin viscous boundary layer over a compliant surface or permeable liner," *Journal of Fluid Mechanics*, vol. 678, pp. 348–378, 7 2011.
[18] D. Khamis and E. J. Brambley, "Viscous effects on the acoustics and stability of a shear layer over an impedance wall," *Journal of Fluid Mechanics*, vol. 810, pp. 489–534, 2017.
[19] E. J. Brambley and G. Gabard, "Time-domain implementation of an impedance boundary condition with boundary layer correction," *Journal of Computational Physics*, vol. 321, no. 321, pp. 755–775, 2016.
[20] D. Khamis and E. J. Brambley, "Acoustic boundary conditions at an impedance lining in inviscid shear flow," *Journal of Fluid Mechanics*, vol. 796, pp. 386–416, 2016.
[21] D. J. Tritton, *Physical Fluid Dynamics*. Oxford University Press, 1988.
[22] Y. Renou and Y. Aurégan, "On a Modified Myers Boundary Condition to Match Lined Wall Impedance Deduced from Several Experimental Methods in Presence of a Grazing Flow," 2010, aIAA Paper 2010-3945.
[23] M. G. Jones, W. R. Watson, and T. L. Parrott, "Benchmark Data for Evaluation of Aeroacoustic Propagation Codes with Grazing Flow," 2005, aIAA Paper 2005-2853.
[24] G. Gabard, "A comparison of impedance boundary conditions for flow acoustics," *Journal of Sound and Vibration*, vol. 332, no. 4, pp. 714–724, February 2013.
[25] M. N. Mikhail and M. R. El-Tantawy, "The acoustic boundary layers: a detailed analysis," *Journal of Computational and Applied Mathematics*, vol. 51, pp. 15–36, 1994.
[26] B. J. Tester, "The propagation and attenuation of sound in lined ducts containing uniform or plug flow," *Journal of Sound and Vibration*, vol. 28, no. 2, pp. 151–203, 1973.
[27] S. W. Rienstra, "Impedance models in time domain, including the extended helmholtz resonator model,"

2006, aIAA Paper 2006-2686.
[28] U. Ingard, "Influence of fluid motion past a plane boundary on sound reflection, absorption, and transmission," *Journal of the Acoustical Society of America*, vol. 31, pp. 1035–1036, 1959.
[29] M. K. Myers, "On the acoustic boundary condition in the presence of flow," *Journal of Sound and Vibration*, vol. 71, no. 3, pp. 429–434, 1980.
[30] E. J. Brambley, "Fundamental problems with the model of uniform flow over acoustic linings," *Journal of Sound and Vibration*, vol. 322, pp. 1026–1037, 2009.
[31] D. Marx and Y. Aurégan, "Effect of turbulent eddy viscosity on the unstable surface mode above an acoustic liner," *Journal of Sound and Vibration*, vol. 332, no. 15, pp. 3803–3820, 2013.
[32] E. J. Brambley, M. Darau, and S. W. Rienstra, "The critical layer in linear-shear boundary layers over acoustic linings," *Journal of Fluid Mechanics*, vol. 710, pp. 545–568, 2012.
[33] H. Beyer and S. Kempfle, "Definition of Physically Consistent Damping Laws with Fractional Derivatives," *Zeitschrift Angewandte Mathematik und Mechanik*, vol. 75, pp. 623–635, 1995.
[34] S. Holm and S. P. Näsholm, "A causal and fractional all-frequency wave equation for lossy media," *The Journal of the Acoustical Society of America*, vol. 130, no. 4, pp. 2195–2202, 2011.
[35] M. J. Carcione, F. Cavallini, F. Mainardi, and A. Hanyga, "Time-domain modeling of constant-q seismic waves using fractional derivatives," *Pure and Applied Geophysics*, vol. 159, no. 7, pp. 1719–1736, 2002.
[36] R. Scherer, S. L. Kalla, Y. Tang, and J. Huang, "The grünwald–letnikov method for fractional differential equations," *Computers & Mathematics with Applications*, vol. 62, no. 3, pp. 902–917, 2011, special Issue on Advances in Fractional Differential Equations II.